The Theory of Ice Nucleation by Heterogeneous Freezing of Deliquescent Mixed CCN. Part II: Parcel Model Simulation

VITALY I. KHVOROSTYANOV

Central Aerological Observatory, Moscow, Russia

JUDITH A. CURRY

School of Earth and Atmospheric Sciences, Georgia Institute of Technology, Atlanta, Georgia

(Manuscript received 15 July 2002, in final form 30 June 2004)

ABSTRACT

The new theory of ice nucleation by heterogeneous freezing of deliquescent mixed cloud condensation nuclei (CCN) presented in Part I is incorporated into a parcel model with explicit water and ice bin microphysics to simulate the process of ice nucleation under transient thermodynamic conditions. Simulations are conducted over the temperature range $-4°$ to $-60°$C, with vertical velocities varying from 1 to 100 cm s^{-1}, for varying initial relative humidities and aerosol characteristics. These simulations show that the same CCN that are responsible for the drop nucleation may initiate crystal nucleation and can be identified as ice nuclei (IN) when crystals form. The simulated nucleation rates and concentrations of nucleated crystals depend on temperature and supersaturation simultaneously, showing good agreement with observations but with noticeable differences when compared with classical temperature-only and supersaturation-only parameterizations. The kinetics of heterogeneous ice nucleation exhibits a negative feedback via water supersaturation, whereby ice nucleation depends on the water supersaturation that is diminished by ice crystal diffusional growth. This feedback is stronger than the corresponding feedback for drop nucleation, and may explain discrepancies between observed ice nuclei concentrations and ice crystal concentrations, the very small fraction of CCN that may serve as IN, and the much smaller crystal concentrations as compared to drop concentrations. The relative importance of heterogeneous versus homogeneous nucleation is examined for a variety of cloud conditions. Based on these calculations, a simple parameterization for ice crystal concentration is suggested for use in cloud models and large-scale models.

1. Introduction

It is well known that droplet nucleation and diffusional growth in natural clouds is a self-regulating process with strong negative feedback. Cloud supersaturation, upon which nucleation and diffusional growth depend, is determined by competition between supersaturation generation by the dynamical and radiative forcing and supersaturation depletion by the nucleated and growing drops. Since the rate of nucleation of cloud drops depends on supersaturation (e.g., as summarized by Pruppacher and Klett 1997, hereafter PK97), nucleation continues only if the rate of supersaturation generation exceeds the rate of its depletion.

Cloud ice crystal nucleation is much more complicated and it is not clear whether any similar supersaturation-dependent mechanism with a negative feedback governs the kinetics of ice crystal nucleation or why crystal concentrations in clouds are three–five orders of magnitude smaller than drop concentrations. Ice nuclei concentration N_{IN} has been parameterized in cloud physics for several decades either as a function of temperature (Fletcher 1962; Young 1974; Meyers et al. 1992), as a function of ice supersaturation (Huffman 1973; Meyers et al. 1992), or as some combination of these two dependencies (e.g., Cotton et al. 1986). The main disadvantage of previous parameterizations of ice nucleation is that they are empirical, with parameters tuned to produce ice crystal concentrations N_c within some limited range of temperatures and supersaturation based on field or laboratory measurements. Such an approach has led to contradictions between parameterizations of the measured concentrations of ice nuclei, N_{IN}, and of the crystals, N_c, so that the "ice enhancement factor" $R_M = N_c/N_{\mathrm{IN}}$, can reach values as high as 10^4–10^5 at $T = -5°$C (e.g., Hobbs 1969; Hobbs et al. 1980), which has produced hypotheses of "ice multiplication" (e.g., Hallett and Mossop 1974) or requirements for high water super-

Corresponding author address: Dr. J. A. Curry, School of Earth and Atmospheric Sciences, Georgia Institute of Technology, Atlanta, GA 30332-0340.
E-mail: curryja@eas.gatech.edu

saturations (Rangno and Hobbs 1991; Hobbs and Rangno 1990).

Supersaturation dependence of ice nuclei concentration may produce a negative feedback and stop nucleation even in the presence of external sources of supersaturation generation; the temperature dependence of ice nucleation does not have this feature. If a source of cooling persists, the latent heat release of growing crystals may hamper nucleation but cannot stop it, commonly producing unrealistically high values of N_i, and artificial methods may be required to prevent unlimited ice nucleation when using a temperature-dependent parameterization (e.g., Spice et al. 1999). The heterogeneous freezing nucleation rate of classical nucleation theory describes the temperature dependence of the nucleation rate but does not contain supersaturation dependence (e.g., PK97). The theory of heterogeneous condensation freezing by Fukuta and Schaller (1982) discussed in Part I showed that a combined temperature–supersaturation dependence occurs if heterogeneous freezing takes place as a two-step process: 1) condensation on insoluble aerosol particles that depends on both temperature and supersaturation as described by the classical theory of condensation on insoluble particles and 2) subsequent freezing that depends on temperature (Fletcher 1962). The resulting isopleths of heterogeneous condensation freezing in Fukuta and Schaller (1982) showed simultaneous dependence of nucleation on both supersaturation and temperature. A similar model for the immersion-freezing mode was considered by Young (1993).

A new theory of ice nucleation by heterogeneous freezing of deliquescent mixed cloud condensation nuclei (CCN) is presented in Khvorostyanov and Curry (2004, hereafter Part I) that describes simultaneously both the temperature and supersaturation dependencies of ice crystal nucleation. Heterogeneous ice crystal nucleation was examined in Part I for static conditions, that is, for fixed temperature and supersaturation. However, nucleation rates and concentration of nucleated crystals cannot be explored and explained without a dynamical framework. Here we incorporate this new theory of ice nucleation by heterogeneous freezing of deliquescent mixed CCN into a parcel model with explicit water and ice bin microphysics to simulate the process of ice nucleation under transient thermodynamic conditions. Simulations are conducted over the temperature range $-4°$ to $-60°$C, with vertical velocities varying from 1 to 100 cm s^{-1}, for varying initial relative humidities and aerosol characteristics. It is shown that the kinetics of heterogeneous ice nucleation exhibits a negative feedback regulated via water supersaturation. This feedback is similar to that found for homogeneous nucleation in works cited here and in Part I (e.g., Lin et al. 2002) and is much stronger than the corresponding feedback for drop nucleation, and may explain discrepancies between observed ice nuclei concentrations and ice crystal concentrations. The relative importance of heterogeneous versus homogeneous nucleation is examined for a variety of cloud conditions, and possible applications of this theory for cloud modeling are discussed.

2. Parcel model

A parcel model with explicit water and ice bin microphysics is formulated to simulate the evolution of cloud microphysical processes in adiabatic ascent. The microphysical formulation used here is similar to the Eulerian numerical 1D, 2D, and 3D models used previously for simulation of mixed-phase Arctic clouds (Khvorostyanov 1995; Khvorostyanov et al. 2001, 2003), with some differences in equations owing to the Lagrangian approach in the parcel model. In the parcel model, vertical velocity is specified. The main thermodynamic equations are the prognostic equations for supersaturation and temperature. This system of equations includes terms that describe the phase transitions and is closed using the kinetic equations of condensation for the drop and ice crystal size distribution functions that account for nucleation and diffusional growth. Following the methodology recommended for the Cirrus Parcel Model Comparison Project (CPMCP; Lin et al. 2002), we deliberately exclude from consideration coagulation among the droplets and aggregation between the droplets and crystals, sedimentation, entrainment, turbulent exchange, etc., to isolate the effects directly related to nucleation processes. The supersaturation and kinetic equations for particle size distributions are described below.

a. Supersaturation equation

In this section, we consider equations for the relative water supersaturation $\delta_w = (\rho_v - \rho_{ws})/\rho_{ws}$ and relative ice supersaturation $\delta_i = (\rho_v - \rho_{is})/\rho_{is}$, where ρ_v is the vapor density, and ρ_{ws} and ρ_{is} are saturated vapor densities over water and ice. The equation for δ_w can be derived from the relation

$$\frac{d\delta_w}{dt} = \frac{1}{\rho_{ws}}\frac{d\rho_v}{dt} - \frac{\rho_v}{\rho_{ws}^2}\frac{d\rho_{ws}}{dt}. \tag{2.1}$$

The term $d\rho_{ws}/dt$ can be expressed via the cooling rate dT/dt using the Clausius–Clapeyron equation:

$$\frac{d\rho_{ws}}{dt} = \frac{d\rho_{ws}}{dT}\frac{dT}{dt} = \frac{\rho_{ws}}{T}\left(\frac{L_e}{R_v T} - 1\right)\frac{dT}{dt}, \tag{2.2}$$

where R_v is the specific gas constant for water vapor and L_e is the specific latent heat of evaporation. The term $d\rho_v/dt$ in (2.1) can be transformed using the continuity equations for air and vapor and the equation of state:

$$\frac{d\rho_v}{dt} = -(I_{\text{dep}} + I_{\text{con}}) + \frac{\rho_v}{p}\frac{dp}{dt} + \frac{\rho_v}{T}\frac{dT}{dt}. \tag{2.3}$$

Here $I_{\rm dep}$ and $I_{\rm con}$ are, respectively, the deposition vapor flux to the crystals and condensation flux to the droplets. Substituting (2.2) and (2.3) into (2.1), we obtain the supersaturation equation:

$$\frac{1}{(1+\delta_w)}\frac{d\delta_w}{dt}=\frac{1}{p}\frac{dp}{dt}-\frac{L_e}{R_v T^2}\frac{dT}{dt}-\frac{I_{\rm dep}+I_{\rm con}}{\rho_v}. \quad (2.4)$$

The term dT/dt can be excluded using the heat balance equation:

$$\rho_a c_p\frac{dT}{dt}=\frac{dp}{dt}+L_e I_{\rm dep}+L_s I_{\rm con}, \quad (2.5)$$

where L_s is the specific sublimation (deposition) latent heat rate. Substituting dT/dt from (2.5) into (2.4), we obtain

$$\frac{1}{(1+\delta_w)}\frac{d\delta_w}{dt}=\frac{1}{p}\frac{dp}{dt}\left(1-\frac{L_e}{c_p T}\frac{M_w}{M_a}\right)-\frac{\Gamma_1 I_{\rm dep}}{\rho_v}-\frac{\Gamma_{12} I_{\rm con}}{\rho_v}, \quad (2.6)$$

where M_w and M_a are the molecular weights for water and dry air and

$$\Gamma_1=1+\frac{L_e^2}{c_p R_v T^2}\frac{\rho_{ws}}{\rho_a},\quad \Gamma_{12}=1+\frac{L_e L_s}{c_p R_v T^2}\frac{\rho_{ws}}{\rho_a}. \quad (2.7)$$

The vapor fluxes to the droplets and crystals are the integrals of the mass growth rates that are expressed via growth rates $\dot r_c$, $\dot r_d$ of the crystal and droplet radii over the corresponding size spectra, where r_c and r_d are corresponding radii:

$$I_{\rm dep}=4\pi\rho_i\int_0^\infty r_c^2\dot r_c f(r_c,t)dr_c=\frac{\rho_{is}\delta_i}{\Gamma_2}\tau_{fc}^{-1}, \quad (2.8a)$$

$$I_{\rm con}=4\pi\rho_w\int_0^\infty r_d^2\dot r_d f(r_d,t)dr_d=\frac{\rho_{iw}\delta_w}{\Gamma_1}\tau_{fd}^{-1}, \quad (2.8b)$$

where Γ_2 is similar to Γ_1 in (2.7) with substitution $L_e\to L_s$. We use $\dot r_c$, $\dot r_d$ in the form (e.g., Sedunov 1974) equivalent to that described, for example, in Young (1993), Lin et al. (2002) and used in many cloud models:

$$\dot r_c=c_{i3}\frac{\delta_i}{r_c+\beta_{\rm dep}},\quad c_{i3}=\frac{D\rho_{is}}{\rho_i\Gamma_2},\quad \beta_{\rm dep}=4D/\alpha_d, \quad (2.9a)$$

$$\dot r_d=c_{w3}\frac{\delta_w}{r_d+\beta_{\rm con}},\quad c_{w3}=\frac{D\rho_{ws}}{\rho_w\Gamma_1},\quad \beta_{\rm con}=4D/\alpha_c, \quad (2.9b)$$

where D is the water vapor diffusivity, α_d and α_c are the deposition and condensation coefficients, and we have introduced the supersaturation relaxation times for the crystals, τ_{fc}, and droplets, τ_{fd}:

$$\tau_{fc}^{-1}=4\pi D\int_0^\infty\frac{r_c^2}{r_c+\beta_c}f_c(r_c,t)dr_c\approx 4\pi D N_c\bar r_c, \quad (2.10a)$$

$$\tau_{fd}^{-1}=4\pi D\int_0^\infty\frac{r_d^2}{r_d+\beta_d}f_d(r_d,t)dr_d\approx 4\pi D N_d\bar r_d. \quad (2.10b)$$

Substituting (2.8a), (2.8b) into (2.6), we obtain the equation for δ_w:

$$\frac{1}{(1+\delta_w)}\frac{d\delta_w}{dt}=\frac{1}{p}\frac{dp}{dt}\left(1-\frac{L_e}{c_p T}\frac{M_w}{M_a}\right)-\frac{1}{\tau_d}\frac{\delta_w}{(1+\delta_w)}-\frac{1}{\tau_c}\frac{\Gamma_{12}}{\Gamma_2}\frac{\delta_i}{(1+\delta_i)}. \quad (2.11)$$

If the cooling rate occurs in a rising parcel with vertical velocity w, then the term with pressure can be expressed using the hydrostatic equation and equation of state as $(1/p)(dp/dt)=-(g/R_a T)w$, where g is acceleration of gravity and R_a is the specific gas constant of the dry air. Substitution of this into (2.11) yields

$$\frac{d\delta_w}{dt}=(1+\delta_w)c_1-\delta_w\left(\frac{1}{\tau_{fd}}+\frac{\Gamma_{12}}{\Gamma_2}\frac{1}{\tau_{fc}}\right)-\frac{\Gamma_{12}}{\Gamma_2}\frac{1}{\tau_{fc}}\frac{\rho_{ws}-\rho_{is}}{\rho_{ws}}, \quad (2.12a)$$

$$c_1(T)=\left(\frac{L_e}{c_p T}\frac{M_w}{M_a}-1\right)\frac{g}{R_a T}w. \quad (2.12b)$$

The first term on the right-hand side of (2.12a) describes the supersaturation generation in the parcel in adiabatic ascent, the second term represents the δ_w absorption by diffusional growth of the droplets and crystals, and the last term arises from the flux from the droplets to the crystals (Bergeron–Findeisen process). Equation (2.12a) can be written in a slightly different form that is more convenient for analytical solutions:

$$\frac{d\delta_w}{dt}=(1+\delta_w)c_1-\delta_w\tau_{fd}^{-1}-c_2\delta_i\tau_{fc}^{-1}, \quad (2.13a)$$

$$c_2(T)=\frac{\Gamma_{12}}{\Gamma_2}\frac{1+\delta_w}{1+\delta_i}, \quad (2.13b)$$

where the functions c_1, c_2 depend on temperature.

b. Kinetic equations for particle size spectra

Evolution of the droplet and crystal spectra is described using two kinetic equations for $f_d(r_d)$ *and* $f_c(r_c)$ (Buikov 1961, 1963):

$$\frac{\partial f_c}{\partial t}+\frac{\partial}{\partial r_c}(\dot r_c f_c)=\psi_{fc}(r_c,t), \quad (2.14a)$$

$$\frac{\partial f_d}{\partial t}+\frac{\partial}{\partial r_d}(\dot r_d f_d)=\psi_{fd}(r_d,t). \quad (2.14b)$$

The source terms ψ_{fc} and ψ_{fd} on the right-hand side describe particle nucleation. The droplet nucleation

term ψ_{fd} can be calculated by introducing the CCN activity spectrum $n(\delta_{w0})$:

$$\psi_{fd} = n(\delta_{w0}) \frac{d\delta_{w0}}{dt} \delta(r_d - r_b), \tag{2.15}$$

where $r_b = (2/3)(B/\delta_{w0})$ is the boundary radius, $B \approx 1.2 \times 10^{-7}$ cm is the Kelvin curvature parameter, and $n(\delta_{w0})$ can be determined from Twomey's power law, derived either from the CCN supersaturation activity spectrum (PK97) or from the CCN size spectrum (e.g., Sedunov 1974; Khvorostyanov and Curry 1999a):

$$n_d(\delta_{w0}) = P_d \delta_{w0}^l. \tag{2.16}$$

The crystal nucleation term can be calculated as

$$\psi_{fc} = \Delta N_c / \Delta t, \tag{2.17}$$

where ΔN_c is the number concentration of the crystals nucleated in time step Δt. The model includes both heterogeneous and homogeneous ice nucleation processes. Heterogeneous nucleation is included following Part I. The homogeneous nucleation rate is determined below.

c. Particle nucleation

Droplet nucleation is calculated using Twomey's power law as $\Delta N_d = C_d \Delta(\delta_w^p)/\Delta t$, where Δ denotes an increase in one time step Δt and C_d is the normalizing constant proportional to the total CCN concentration N_a and related to its soluble fraction and microstructure as described in Khvorostyanov and Curry (1999a). Since δ_w (in %) is substantially less than 1% during drop activation, $N_d < N_a$. If δ_w reaches 0 and increases, then $\psi_{fd} = \Delta N_d / \Delta R_d / \Delta t$ and the new drops are placed in the first size bin ΔR_d of $f_d(r_d)$.

The crystal source term is calculated for the heterogeneous deliquescent-freezing mode as $\psi_{fc} = \Delta N_{fr}/\Delta R_c/\Delta t$ with the number ΔN_{fr} of the crystals nucleated on frozen CCN–IN in a time step Δt calculated from (4.5) of Part I. Here ΔR_d, ΔR_c, denote the first size steps by the droplet and crystal radii (0.1–1 μm). Both spectra include 30 points by radius: 10 steps by 0.1–1 μm and the next 20 steps increasing logarithmically to 350 μm. The experiments showed that this division allows coverage of both small and large size ranges without losing accuracy.

In section 4, we compare the heterogeneous and homogeneous ice nucleation modes. The homogeneous nucleation rate J_{hom} [cm^{-3} s^{-1}] is determined via (PK97):

$$J_{\text{hom}} = C_{\text{hom}} \exp\left(- \frac{\Delta F_{\text{act}} + \Delta F_{g,\text{hom}}}{kT} \right),$$

$$C_{\text{hom}} = 2N_0 \left(\frac{\rho_w kT}{\rho_i h} \right) \left(\frac{\sigma_{is}}{kT} \right), \tag{2.18}$$

where ΔF_{act} is the activation energy for diffusion across the liquid–ice boundary, $\Delta F_{g,\text{hom}}$ the critical energy of ice germ formation, ρ_w the density of water, k and h the Boltzmann's and Planck's constants, σ_{is} the surface tension at the ice and solution interface, N_0 the number of molecules in contact with a unit area of ice, and T the droplet temperature. Analytical expressions for the critical germ radius r_{cr} and $\Delta F_{g,\text{hom}}$ with account for solution and curvature effects were derived in Khvorostyanov and Sassen (1998a, hereafter KS98, 2002) in a manner similar to Khvorostyanov and Curry (2000, hereafter KC00) and Part I, by integrating the condition of equilibrium for the three-phase system: water vapor, and an aqueous solution (haze particle) containing an ice germ, but without an insoluble substrate inside the drop. The equation for r_{cr} is the same as (2.7) in Part I, and the equation for $\Delta F_{g,\text{hom}}$ coincides with the first term on the right-hand side of (2.10) for ΔF_{cr} in Part I with $\varepsilon = 0$, $f(x, m_{is}) = 1$ ($m_{is} = -1$). The surface tensions and latent heat were taken from PK97, and ΔF_{act} was fitted to the data from Jeffery and Austin (1997) obtained from the new equation of state.

3. Simulation results

To simulate the ice crystal nucleation process, the parcel model was run for 1–3 hours, varying the initial temperature (T_{0c}), relative humidity (RHW_0), vertical velocity (w), and aerosol characteristics. The only two additional parameters of this model of heterogeneous freezing are the relevant aerosol characteristics (see Part I): the misfit strain ε and the wetability or contact parameter, m_{is}. Most runs were performed with $\varepsilon = 0$, and sensitivity to $\varepsilon = 1\%$–2% was tested in some experiments. The parameter m_{is} given in Table 5.2 in PK97 for surface soil ($m_{is} = 0.36$–0.42) and quartz ($m_{is} = 0.63$–0.72) might be representative for mixed CCN. Kärcher et al. (1996) recently measured the values $m_{is} = 0.44$–0.57 for soot that may constitute an insoluble carbonaceous fraction of IN. Therefore the average values of $m_{is} = 0.50$ or 0.52 were taken in the simulations described in detail below. The sensitivity to the lower and higher values in the range 0.12–0.75 was also tested. Numerical experiments showed that the values of m_{is} are mostly limited to this rather narrow range, otherwise freezing occurs too rapidly (for $m_{is} \geq 0.67$) or slowly (for small $m_{is} \leq 0.40$). This is caused by the exponential dependence of nucleation rate $J_{s,\text{fr}}$ on $\Delta F_{\text{cr}} \sim f(m_{is}, x)$, emphasized by Fletcher (1962) and discussed in Part I.

The model includes the option of isolating specific ice crystal nucleation modes by turning off the other modes. In this study we deal with heterogeneous and homogeneous freezing of deliquescent CCN, and the other modes (deposition, contact, immersion) are not considered. The initial pressure p_0 is specified in most runs to be 800 hPa. The CCN concentration typical for continental clouds $N_a = 500$ cm^{-3} (PK97) is chosen for all runs except for simulation of ice nucleation in maritime convective clouds, where $N_a = 100$–150 cm^{-3}, and

for comparison of heterogeneous and homogeneous modes in cirrus clouds at low T and high altitudes, where $N_a = 200\ \text{cm}^{-3}$ as was recommended and used in CPMCP (Lin et al. 2002). Several experiments were performed with $N_a = 50$–$100\ \text{cm}^{-3}$ at $T = -20°\text{C}$ to $-30°\text{C}$ to test the possibility of mixed-phase cloud existence at these temperatures. The insoluble aerosol size spectrum over r_N is lognormal with modal radius $r_m = 0.02\ \mu\text{m}$ and dispersion $\sigma = 2.5$; at $\delta_w > 0$, it is limited by the boundary radius r_b as described in Part I. More than 300 simulations were performed with variable combinations of T_0, RHW_0, m_{is}, ε, w, aerosol microstructure, and the mode of freezing (heterogeneous deliquescent-freezing and/or homogeneous freezing).

The time steps were 0.01–0.2 s in the main program, but the time step can be divided further in the condensation subroutines to meet the stability condition $\Delta t \ll \min(\tau_d, \tau_c)$. The accuracy of the calculations was controlled by comparing the total number of crystals nucleated with those obtained by integration over the size spectrum of the grown crystals at the end of a parcel run. If the error exceeded 5% (especially at low temperatures), the time and radius steps were varied and several additional runs were performed until the error became less than 5%. The runs with vertical velocities $w = 1$–$5\ \text{cm s}^{-1}$ described in section 3 were conducted for a period of 3 h, which was sufficient to trace all stages of supersaturation growth, nucleation, and subsequent supersaturation relaxation. In the runs with higher $w = 30$–$100\ \text{cm s}^{-1}$ all processes are faster, and it was sufficient to conduct simulations for 0.5–1 h. Simulation at cold cirrus temperatures described in section 4 required small time steps and the simulations were conducted for 1 h. The simulation results are described below.

a. Kinetics of ice nucleation in the mixed and crystalline clouds with weak updrafts

In this section, we describe the temporal evolution of the ice nucleation process. Presented in Figs. 1–4 are the results of the run with the initial $T_0 = -14°\text{C}$, $\text{RHW}_0 = 89\%$ ($\delta_w = -11\%$), vertical velocity $w = 2\ \text{cm s}^{-1}$ (which corresponds to a cooling rate of $-0.7°\text{C h}^{-1}$), and $m_{is} = 0.52$. The initial supersaturation over ice is $\delta_i = 11\%$. Figures 1 and 2 illustrate that the temporal evolution can be separated into three stages. During the first stage (up to 115 min), the temperature decreases due to cooling and RHW increases (Figs. 1a,b), which causes a decrease in the critical radius r_{cr} and energy ΔF_{cr} defined in Part I (Figs. 1c,d). During the second stage, starting at $t = 115$ min, the nucleation rates reach their threshold values and grow very rapidly (Figs. 1e,f). At $t = 117$ min, RHW reaches and exceeds 100%, and drop activation occurs. Until $t = 145$ min, δ_w slightly decreases because of the drop formation and growth, and r_{cr} and ΔF_{cr} decrease, while $J_{s,\text{fr}}$ and dN_c/dt increase. Note that this occurs not at the threshold humidity RHW_{th}, but when RHW exceeds the threshold by ~13% (Fig. 1b), in agreement with estimations of the critical saturation ratio $S_{w,\text{cr}}$ in Part I. Ice nucleation rates are noticeable only for about 25 min, when the drops and crystals coexist (Fig. 2). During the third stage (starting nominally at $t = 145$ min), the rate of vapor absorption by the crystals increases sufficiently for complete evaporation of the drops by Bergeron–Findeisen mechanism (Figs. 2d,f). Drops evaporate, RHW abruptly decreases, and r_{cr} and ΔF_{cr} increase rapidly, causing $J_{s,\text{fr}}$ and dN_c/dt to decline below the threshold values and, hence, nucleation stops.

Evolution of the integral characteristics over these three stages of nucleation is shown in Fig. 2. During the first stage, the initial subsaturation δ_w decreases due to cooling and reaches -0.3% at $t = 115$ min (Fig. 2a) when the crystal formation starts (Figs. 2c,e,g), and crystal concentration N_c reaches $\sim 1\ \text{L}^{-1}$ in 5 min by $t = 120$ min. However, since the crystal supersaturation relaxation time is greater than 2 h (Fig. 2b), the crystals cannot absorb all available vapor, and supersaturation generation is still faster than its absorption, so δ_w continues to increase and becomes positive at $t \approx 120$ min. During the second stage, water supersaturation becomes positive, droplets begin to form at $t = 118$ min (Figs. 2d,e,h). Their relaxation time is a few seconds (Fig. 2b), thus the supersaturation generation and absorption are balanced, δ_w does not grow, and drops and crystals coexist for 30 min in a mixed cloud. Meanwhile, crystal nucleation is continuing, N_c reaches $\sim 8\ \text{L}^{-1}$, and the mean radius is 60 μm by $t = 145$ min. The crystal absorption capability gradually increases during the second stage and finally exceeds the rate of supersaturation generation. The vapor flux is directed now from the droplets to the crystals and, due to the intensive Bergeron–Findeisen process, the drops evaporate fast and disappear at $t = 150$ min, when δ_w becomes negative. The crystal concentration continues to increase during the second stage (although at slower rate) and reaches $17.6\ \text{L}^{-1}$ at the end of the second stage. The third stage starts when both δ_w and δ_i begin to decrease. This stage is characterized by constant N_c, but the crystal radius and ice water content (IWC) still increase since δ_i is positive.

Thus the modeled cloud in this example is pure crystalline in the first stage (115–120 min), has mixed-phase structure during the second stage for 30 min, and is again pure crystalline in the third stage. In this case the cloud phase is governed by the relative humidity, which determines also the IN concentration (assuming that $N_{\text{IN}} = N_c$). As water saturation is reached, there is a competition between nucleation of the drops and crystals on the same population of the haze particles that serve at the same time as CCN and IN.

This simulation produced a value of $N_d = 160\ \text{cm}^{-3}$ out of a total $N_{\text{CCN}} = 500\ \text{cm}^{-3}$ CCN. We can define "condensation efficiency" of CCN in producing droplets as $E_{dr} = N_d/N_{\text{CCN}}$, and it is here $E_{dr} \approx 0.32$. The crystals are nucleating simultaneously, and only a very

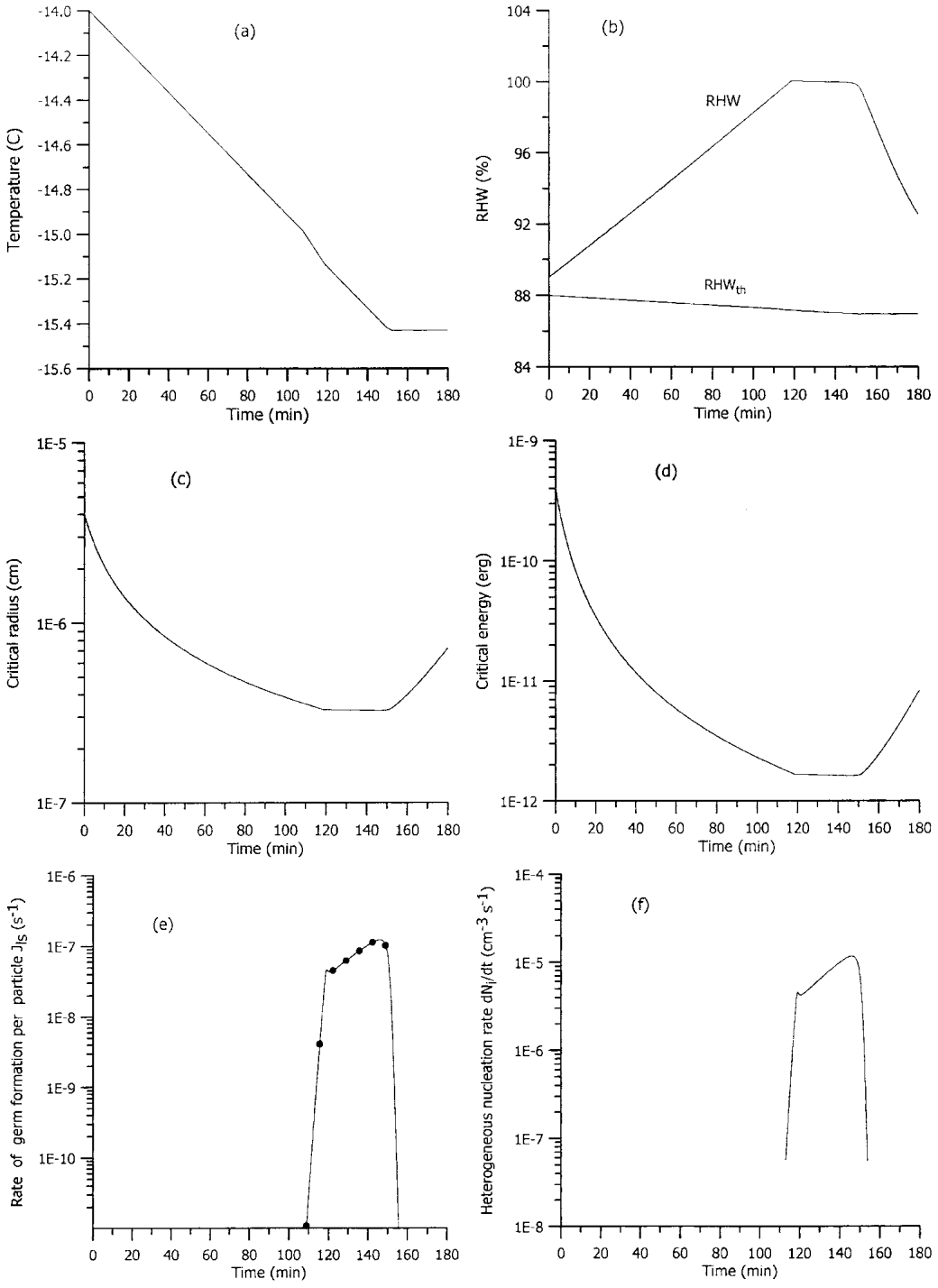

FIG. 1. Temporal evolution of the characteristics of heterogeneous nucleation at $T_0 = -14°C$, $RHW_0 = 89\%$, $w = 2$ cm s^{-1}, $m_{is} = 0.52$. (a) Temperature in the parcel, T, °C; (b) RHW and threshold humidity RHW_{th}, %; (c) germ critical radius, r_{cr}, cm; (d) germ critical free energy, erg; (e) the rate of germ formation per particle $J_{s,fr}$, s^{-1}; (f) polydisperse nucleation rate dN_{fr}/dt, cm^{-3} s^{-1}.

small fraction of the available CCN, 18 L^{-1} ($\sim 2 \times 10^{-2}$ cm^{-3}), was nucleated and would have been identified as IN in chamber experiments. A similar "freezing efficiency" of deliquescent CCN in producing crystals can be defined as $E_{cr} = N_c/N_{CCN} \sim N_{IN}/N_{CCN} = 2 \times 10^{-2}/500 = 40 \times 10^{-6}$. This estimate is close both conceptually and quantitatively to that obtained by Rogers et al. (2001) in recent measurements of IN in the Arctic

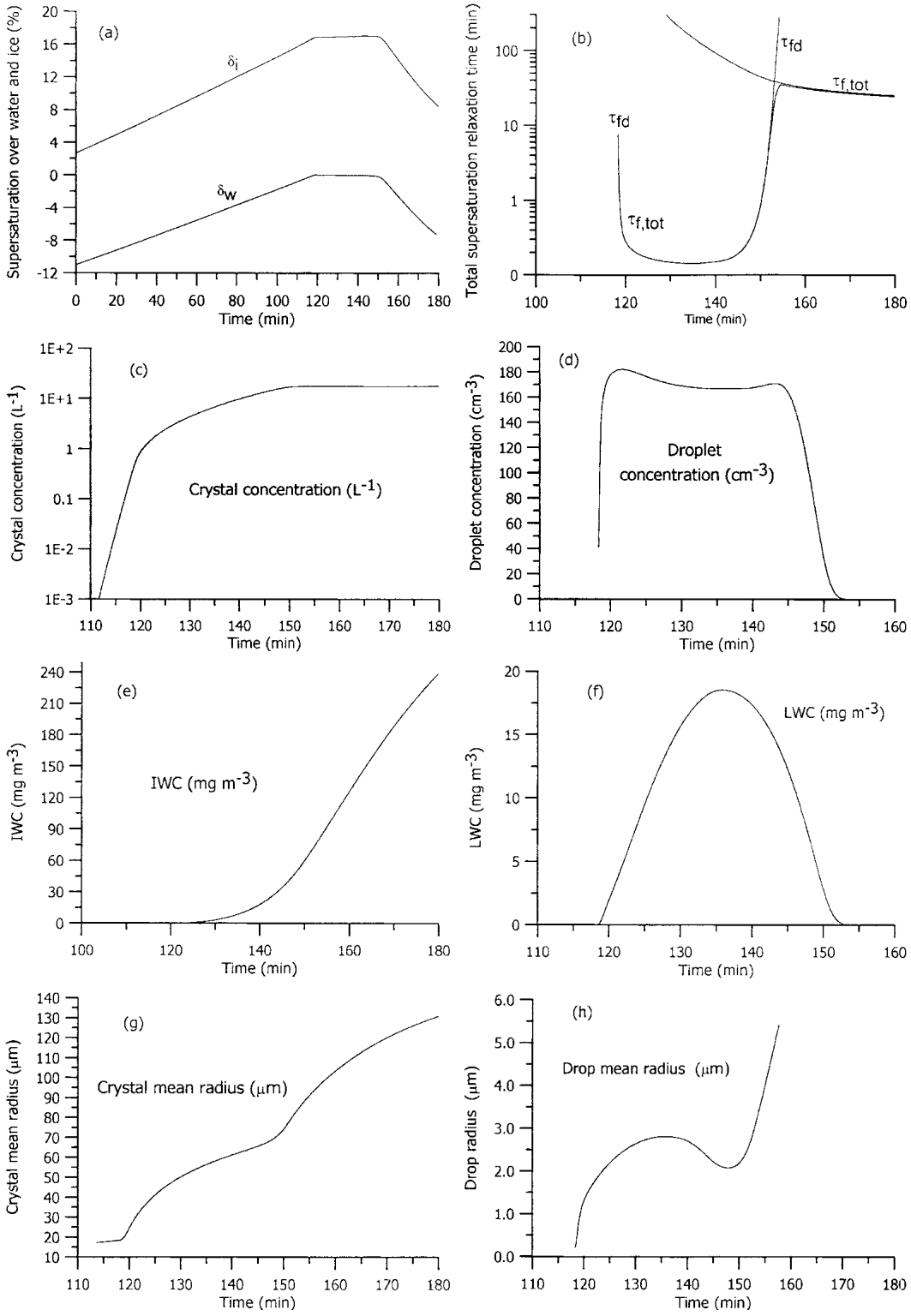

FIG. 2. Temporal evolution of droplet and crystal microphysical properties for the same case as in Fig. 1: $T_0 = -14°C$, RHW = 89%, $w = 2$ cm s^{-1}, $m_{ix} = 0.52$. (a) Supersaturations over water, δ_w, and ice, δ_i, %; (b) supersaturation relaxation times of the droplets, τ_{fd}, crystals, τ_{fc}, and the total relaxation time, $\tau_{f,\text{tot}}$, min; (c) crystal concentration, L^{-1}; (d) droplet concentration, cm^{-3}; (e) ice water and (f) liquid water content, mg m^{-3}; (g) crystal mean radius, μm; and (h) droplet mean radius, μm.

($N_{IN}/N_{CCN} \sim 20 \times 10^{-6}$), in the Subsonic Aircraft: Contrail and Cloud Effects Special Study (SUCCESS; Chen et al. 1998; Rogers et al. 1998), and to the estimates of N_{IN}/N_{CCN} in the parcel model by DeMott et al. (1998).

Since the freezing efficiency E_{cr} of CCN is much less than the condensation efficiency E_{dr}, these results show that the present theory enables explanation of the observed differences between concentrations of the drops and crystals nucleated from the same population of deliquescent mixed CCN similar to the concepts derived from the field experiments (Hobbs and Rangno 1990; Rangno and Hobbs 1991) and developed in the CSU model (DeMott et al. 1998). In numerical experiments here, ice nucleation on the CCN is prevented by a very strong humidity dependence of r_{cr}, ΔF_{cr}, $J_{s,fr}$, and dN_c/dt. The dependence on humidity is an exponential function (see Part I) that is much stronger than the power law for drop nucleation (2.16), which is why crystal nucleation on CCN creates such a strong negative feedback via relative humidity and leads to such dramatic differences between concentrations of drops and crystals.

The dissimilarity between the drops and crystals nucleation on CCN and the ratio of the final concentrations N_c and N_d in a mixed cloud can be illustrated from the analysis of the supersaturation equation (2.11) and Fig. 2. The last two terms in (2.11) are proportional to the vapor fluxes to the drops and crystals and describe supersaturation absorption by the drops and crystals. We denote them as q_w and q_i, and note that according to (2.8)–(2.11), $q_w \sim \delta_w/\tau_d \sim \delta_w N_d r_d$, and $q_i \sim \delta_i/\tau_c \sim \delta_i N_c r_c$. Ice nucleation begins and proceeds at slow nucleation rates, and $q_i \ll q_w$. Activation of drops occurs at $\delta_w \sim 0.1\%$, and during most of the time of liquid phase existence, supersaturation generation by w is balanced mostly by its absorption by the drops (q_w). After drop activation, $\delta_i \sim 20\%$, the newly nucleated crystals grow much faster than the drops and reach larger sizes, $r_i \sim 20$–$30\ r_d$ by the end of cloud glaciation. At this time, supersaturation absorption by the crystals q_i become comparable to q_w and then exceeds it, which causes the decrease of δ_w and ceases ice nucleation (after 150 min in Fig. 2). Therefore we can estimate the ratio of final concentrations N_c and N_d from the condition $q_w \approx q_i$, or $\delta_w N_d r_d \sim \delta_i N_c r_c$, which yields in the above example $N_c/N_d \sim (\delta_w/\delta_i)(r_d/r_c) \sim (0.5 \times 10^{-2})(3 \times 10^{-2}) = 1.5\ 10^{-4}$, in agreement with the simulated $N_c/N_d = 21\ L^{-1}/160\ cm^{-3} = 1.3 \times 10^{-4}$.

Thus, the following factors determine the large difference between concentrations of the crystals and drops formed on the same population of CCN. Crystal nucleation rate dN_c/dt is much slower than that for the drops. Ice supersaturation is $\sim 10^2$–10^3 times greater than water supersaturation in a mixed cloud and this dissimilarity determines the difference in growth rate, sizes, and supersaturation absorption by drops and crystals. Therefore the absorption of supersaturation by crystals begins to exceed its generation by updrafts at much smaller concentrations but larger radii than that for the drops, causing supersaturation to decrease and cessation of ice nucleation at $N_c \ll N_d$.

Note that the value of $J_{s,fr}$ is very small ($<2 \times 10^{-7}\ s^{-1}$) at all stages of the process (Fig. 1e) so that the expressions introduced in Part I can be substantially simplified since

$$\exp\left[-\int_0^t J_{s,fr}(r_N, t')dt'\right] \approx 1 - \int_0^t J_{s,fr}(r_N, t')dt'. \quad (3.3)$$

The probability of freezing $P_{cf}(r_N,t)$ of an aerosol particle with r_N can be written now as

$$P_{cf}(r_N, t) = 1 - \exp\left[-\int_0^t J_{s,fr}(r_N, t')dt'\right] \approx \int_0^t J_{s,fr}(r_N, t')dt'. \quad (3.4)$$

The total number of crystals is obtained by integrating over the aerosol size spectrum:

$$N_{fr}(t) = \int_{r_{min}}^{r_{max}} P_{cf}(r_N, t) f_a(r_N) dr_N \approx \int_{r_{min}}^{r_{max}} \int_0^t J_{s,fr}(r_N, t') f_a(r_N) dt' dr_N. \quad (3.5)$$

The crystal nucleation rate in a polydisperse aerosol [Eq. (4.5) in Part 1] can be simplified as

$$R_{fr}(t) = \frac{dN_{fr}}{dt} = \int_{r_{min}}^{r_{max}} f_a(r_N) J_{s,fr}(r_N, t) dr_N. \quad (3.6)$$

These simplifications can be very useful for analytical estimations and for numerical modeling since they significantly shorten the number of arithmetic operations.

A key issue in heterogeneous nucleation is the contribution of the various regions of aerosol size spectra to the nucleation. Figure 3 shows the subintegral functions of (4.5) and (4.3) in Part I [similar to (3.6) and (3.5) here] for the polydisperse nucleation rate $dN_c/dt(t)$ and crystal concentration $N_c(t)$, illustrating the size contributions to these quantities. The maximum contributions come from the region $r_a \sim 0.1$–$0.6\ \mu m$, in agreement with the available experimental data that show maximum occurrence of the IN radii $\sim$0.2–2.5 μm (e.g., PK97, p. 327) or 0.18–0.23 μm (Rogers et al. 1998, 2001; Chen et al. 1998). Note that we accounted here only for aerosols with $r_N < 4\ \mu m$. It would be interesting to estimate the contributions from larger particles. Berezinsky and Stepanov (1986) showed that these particles (up to 100 μm) might give contributions at higher T (in agreement with Part I) and explained their action by the easier dissolution of the hygroscopic fraction of these IN; an account for such large IN requires knowl-

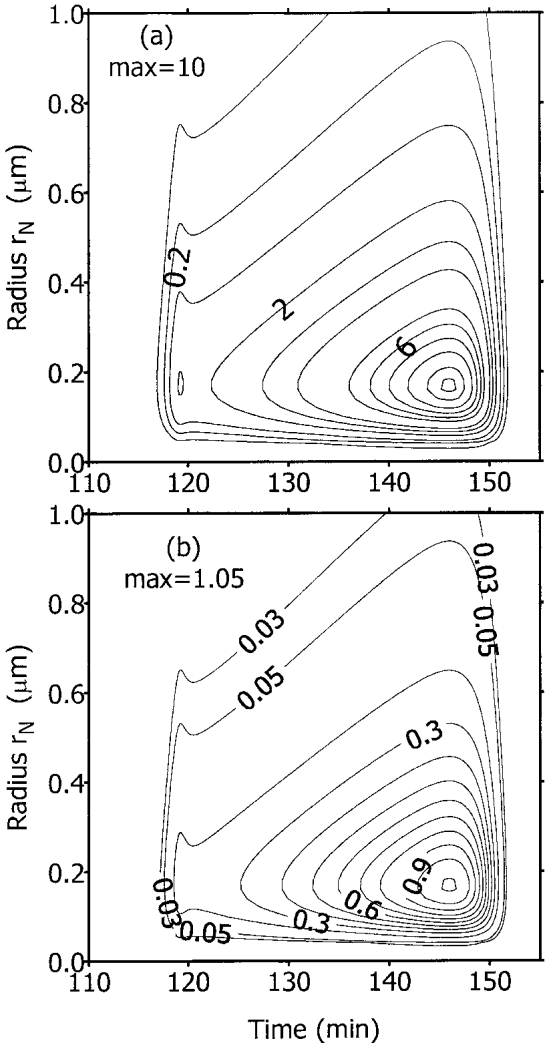

FIG. 3. Characteristics of contributions of various aerosol size fractions into the polydisperse nucleation rate at various stages of nucleation. (a) Subintegral function in polydisperse nucleation rate dN_{fr}/dt (r_N,t), Eq. (4.5) in Part I or Eq. (3.6) here (10^{-7} cm^{-3} s^{-1}); (b) subintegral function in polydisperse concentration N_f (r_N,t) of frozen aerosol, Eq. (4.3) in Part I and Eq. (3.5) here (cm^{-4}). Maxima of subintegral functions are indicated at top.

edge of the distribution of soluble and insoluble fractions inside the large CCN.

The temporal evolution of the ice crystal size spectra is shown in Fig. 4. The maximum crystal radius grows until t = 150 min, corresponding to increasing N_c (see Fig. 2). Nucleation ceases after 150 min, the small size fraction vanishes, the minimum radius at 180 min is 50 μm, and the sizes increase with time. The absolute dispersion of the size spectra σ_{abs} decreases due to the Maxwellian $1/r_i$ growth law, and the relative dispersions $\sigma_{\text{abs}}/r_{i,\text{mean}}$ decreases even faster because of the increasing mean radius $r_{i,\text{mean}}$. Thus, the crystal size spectra produced by a parcel model narrow with time similar to the droplet spectra in response to diffusional growth (PK97). In a real cloud, the spectral narrowing is overwhelmed by turbulence, accretion, and other effects (e.g., Khvorostyanov and Curry 1999b,c).

When the initial temperature decreases further (from −18° to −57°C), no drops occur with m_{is} = 0.5 and the cloud is entirely crystalline, even initially. The kinetics of this process at T_0 = −18°C and w = 2 cm s^{-1} is shown in Fig. 5. The crystals form via heterogeneous freezing of deliquescent CCN at water subsaturations similar to homogeneous freezing but at higher temperatures due to the catalyzing effect of insoluble fraction. The maximum supersaturations over water, δ_{wm}, and over ice, δ_{im}, at which ice nucleation occurs are −3% and 20%, respectively, at T = −19°C, and final N_c = 27 L^{-1}. This case illustrates how clear-sky crystal precipitation (diamond dust) may occur due to deliquescent CCN heterogeneous freezing even at relatively warm temperatures and humidities intermediate between water and ice saturation, such as been observed in the Arctic particularly near open leads with large relative humidity (Ohtake et al. 1982; Curry et al. 1990; Pinto et al. 2001).

A very cold case at T = −54.6°C and w = 2 cm s^{-1} is presented in Fig. 6. The crystal formation occurs at δ_{wm} = −20.4%, final concentration is 76 L^{-1}, IWC increases slowly with time and is 15 mg m^{-3} after 3 h of simulation, with mean crystal radius of 35 μm. This case may correspond to the initial stage of cirrus cloud development. Note that crystal concentration is not very high and matches those measured in cirrus (e.g., Heymsfield and McFarquhar 2002).

Thus, this theory of heterogeneous crystal nucleation describes evolution of the cloud phase structure with lowering temperature and is in general agreement with

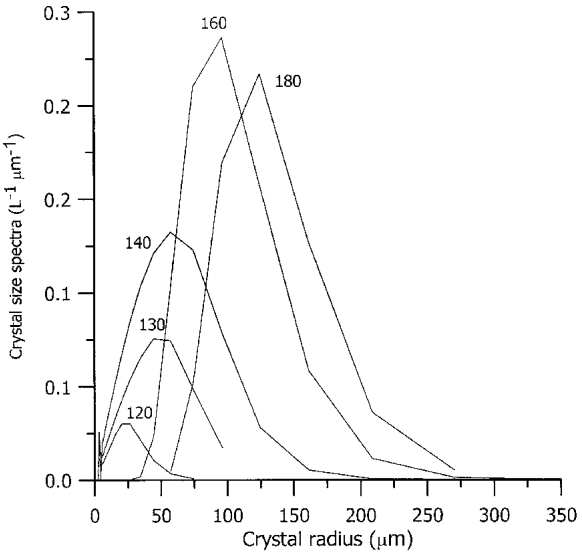

FIG. 4. Temporal evolution of the crystal size spectra for the same conditions as in Figs. 1–3 (T_{0c} = −14°C). The numbers at the curve peaks indicate time in min.

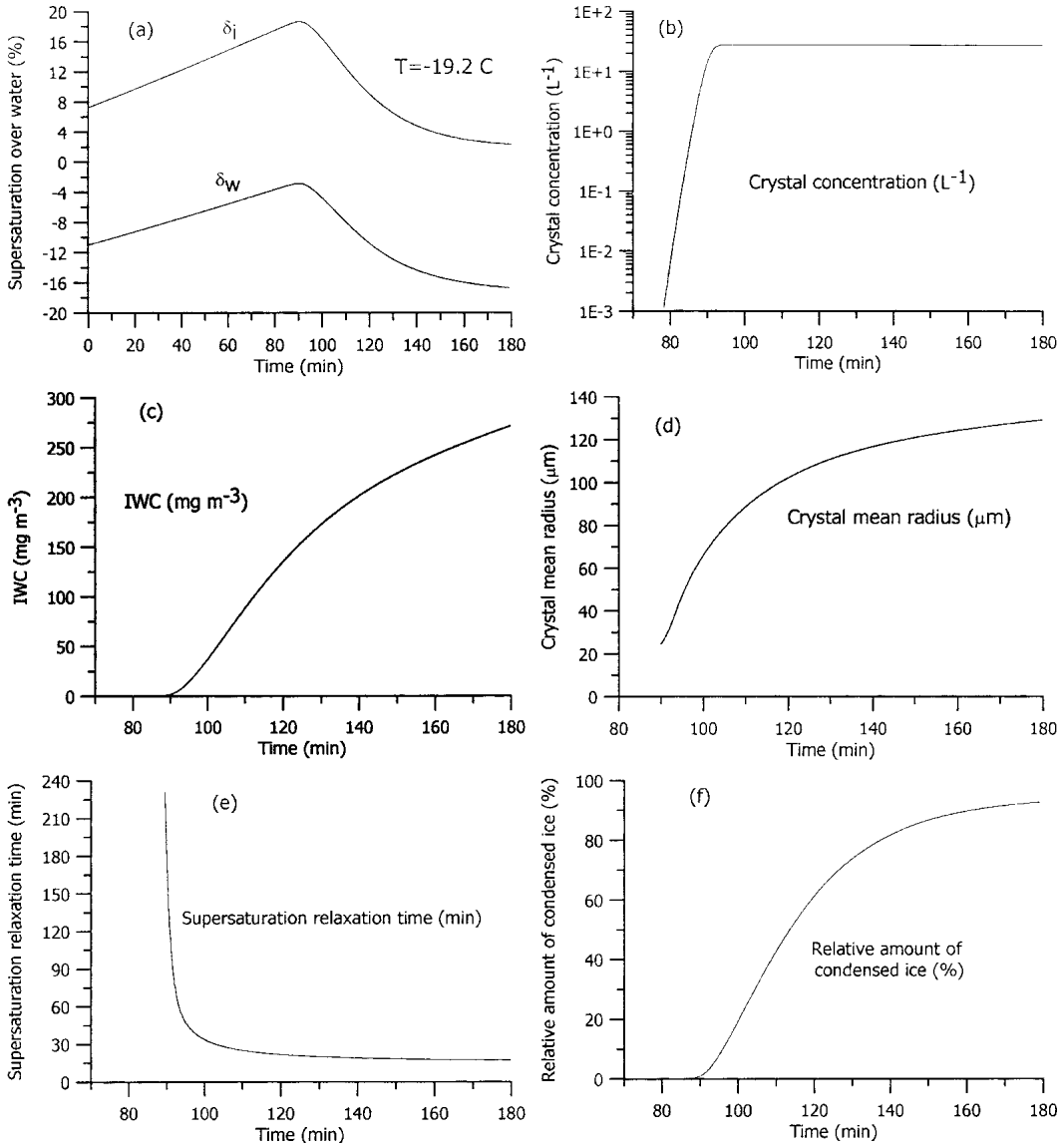

FIG. 5. Temporal evolution of ice crystal microphysical properties with $T_0 = -18°C$, $RHW_0 = 89\%$, $w = 2$ cm s^{-1}, $m_{is} = 0.52$. (a) Supersaturations over water, δ_w, and ice, δ_i, %; (b) crystal concentration, L^{-1}; (c) ice water content, mg m^{-3}; (d) crystal mean radius, μm; (e) crystal supersaturation relaxation time, min; (f) relative amount of condensed ice, %.

observations of cloud phase, which show the occurrence of the ice phase and mixed clouds mostly at $T < -10°C$ and substantial decrease (below 10%) of occurrence of the liquid phase in clouds below $-20°C$ (e.g., PK97, Fig. 2.33).

Figure 7 illustrates the effect of the misfit strain at $T_{0c} = -14°C$. With $\varepsilon = 0$, the drops form at $t \approx 30$ min, crystals form at $t = 30$–75 min with maximum $N_c = 63$ L^{-1}, they coexist in a mixed-phase cloud until 75 min, after which time the drops evaporate, the cloud completely glaciates, water supersaturation decreases, and ice nucleation ceases. With $\varepsilon = 1\%$, ice nucleation begins 15 min later and proceeds slowly until about 2 h. Its rate then becomes comparable with the case $\varepsilon = 0$ and then exceeds it after $t = 2$ h with maximum $N_c = 180$ L^{-1} due to the lower temperature of nucleation, causing full crystallization by 150 min (recall that the parcel retains all particles, although in a real cloud precipitation would occur and the concentration would be much smaller). Because of the slower CCN freezing and Bergeron–Findeisen process in the run with $\varepsilon = 1\%$, maximum liquid water content is 4 times greater than in the case with $\varepsilon = 0$. The case with $\varepsilon = 2\%$ demonstrates the complete absence of crystallization since the threshold $\delta_{w,th}$ is not reached. This strong effect of the misfit strain indicates the necessity of laboratory measure-

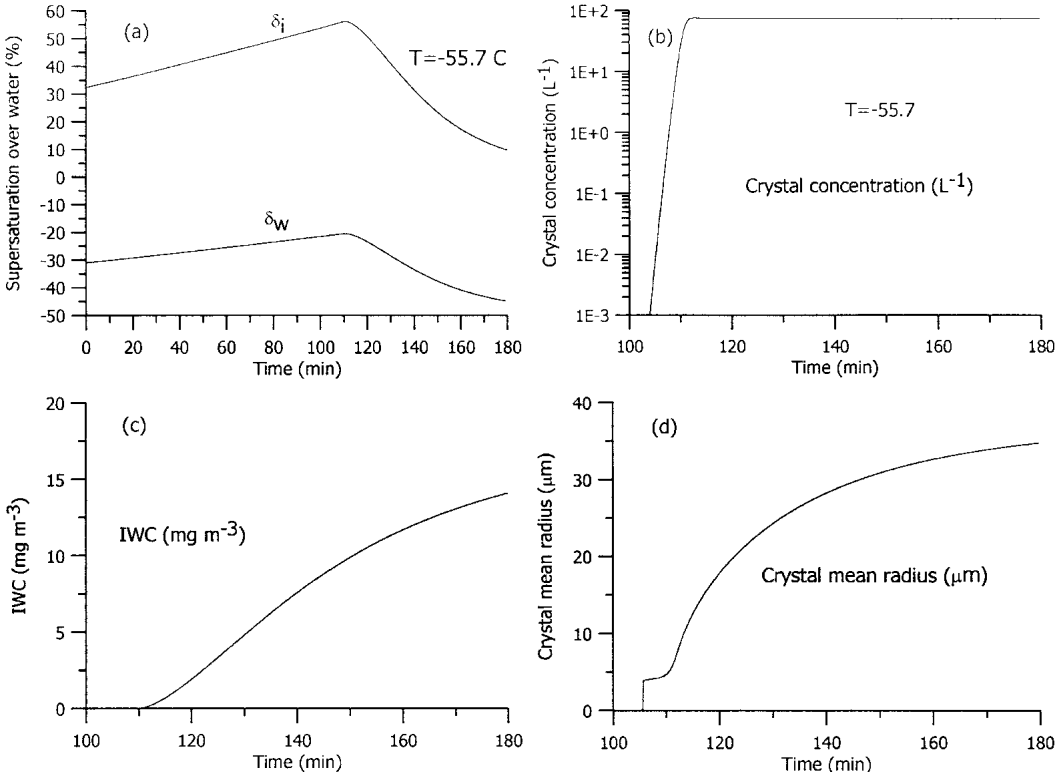

FIG. 6. Time dependence of crystals microphysical properties with $T_0 = -54°C$ (as could be in cirrus), RHW = 69%, $w = 2$ cm s^{-1}, $m = 0.52$. (a) Supersaturations over water, δ_w, and ice, δ_i, %; (b) crystal concentration, L^{-1}; (c) ice water content, mg m^{-3}; (d) crystal mean radius, μm.

ments of the composition, chemical, and crystallographic properties of the aerosol particles.

b. *An estimate of the ice nucleation effects with stronger updrafts*

Hobbs and Rangno (1990, hereafter HR90), Rangno and Hobbs (1991, hereafter RH91) observed very rapid glaciation in maritime cumulus clouds when crystal concentrations increased from ≤ 1 L^{-1} to 300–1100 L^{-1} at warm temperatures of about $-5°$ to $-10°$C over a period of 9 to 15 min. Their analyses showed that the known mechanisms of ice multiplication could not explain the rapid rate of crystal production under the observed conditions. They hypothesized that 1) localized pockets of high water supersaturation of 5%–10% may occur in a cloud after the stage of coalescence and 2) the less effective CCN, not activated at the first stage of cloud development, may be activated in these pockets and serve as condensation freezing or deposition ice nuclei, causing rapid crystal nucleation. Rogers et al. (1994) performed simulations of such situations with a parcel model over a range of vertical velocities from 1 to 10 m s^{-1} and using parameterizations of IN concentration based on chamber experiments. A high water supersaturation and crystal concentration at $T = -15°$C and $w = 3$ m s^{-1} was found just in 1 run of a total of 18, and the authors concluded that such a case may occur only under very specific conditions: with very low drop concentration (supermaritime CCN spectrum), high vertical velocities, and long duration adiabatic parcel ascent. Thus, this study raised the following issues: the probability of such high supersaturations in clouds, whether such supersaturations are required for high crystal concentrations, and whether there are other possible mechanisms of high crystal concentrations and nucleation rates.

We attempted to reproduce the rapid ice crystal nucleation observed by HR90 and RH91 using the CCN deliquescence-freezing model described here, which is in general agreement with the hypothesis from HR90 and RH91 on the role of CCN as IN. Since simulation of the whole life cycle of a convective cloud with an isolated parcel is a risky task, we tried to reproduce a glaciation stage of this process under conditions similar to those observed. From the data in HR90 on cloud-top growth and aircraft pass altitudes, the vertical velocity can be estimated as $w \sim 0.5$–0.8 m s^{-1} at this stage. We performed several simulations with $w = 0.5$–1.0 m s^{-1}.

Figure 8 shows the results of the 1-h simulation with average $w = 65$ cm s^{-1}, RH$W_0 = 0.82$, $T_0 = 0°$C, $m_{is} = 0.5$, $\alpha = 0.2 \times 10^{-5}$ [the surface fraction of an active site, see Fletcher (1969) and Part I], and maritime CCN concentration $N_a = 150$ cm^{-3}. With these parameters,

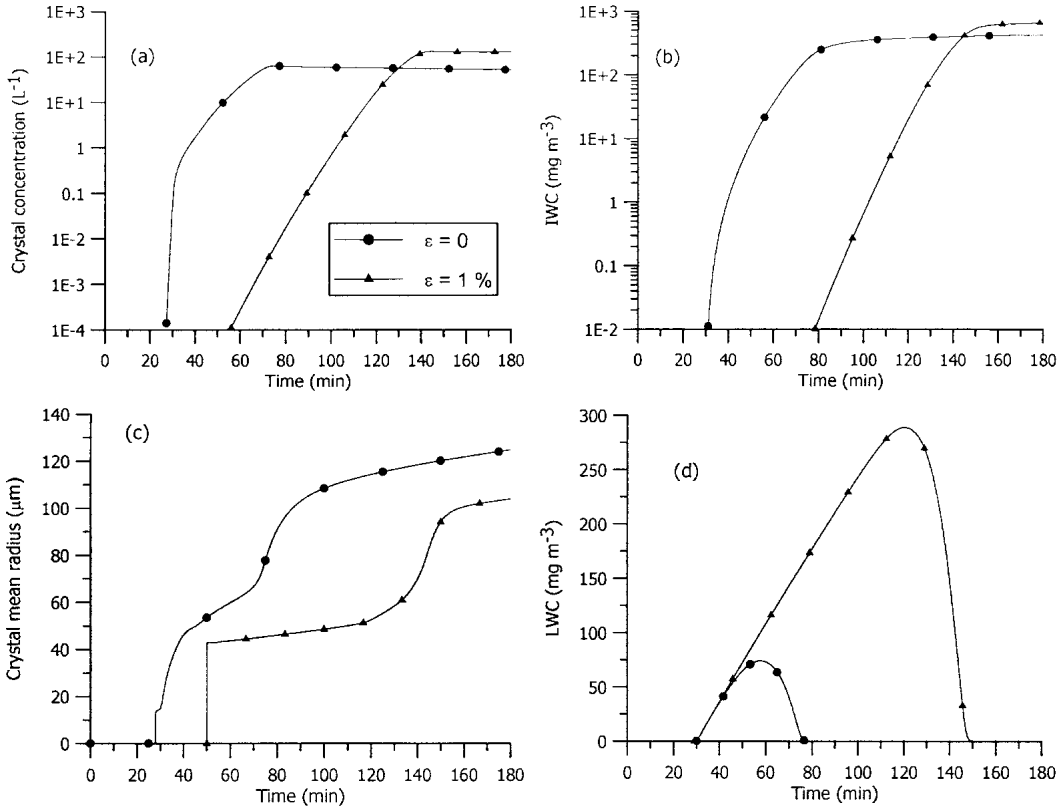

FIG. 7. Comparison of the time evolution of cloud microphysical properties with $T_{0c} = -14°C$, RHW = 89%, $w = 5$ cm s^{-1}, $m = 0.52$ in deliquescence-freezing mode with $\varepsilon = 0\%$ (circles) and $\varepsilon = 1\%$ (triangles). (a) Crystal concentration, L^{-1}; (b) ice water content, mg m^{-3}; (d) crystal mean radius, μm; (d) liquid water content, mg m^{-3}.

condensation begins at 7 min and drop concentration is 92 cm^{-3} (Fig. 8c), similar to HR90 during the passes 1–6 (90–120 cm^{-3}). Crystal nucleation begins at 10 min ($T \approx -4°C$), but concentration is low, ~0.1–0.3 L^{-1}; nucleation accelerates at $t \sim 20$ min, and N_c increases from 1 to 290 L^{-1} from 20 to 33 min (Fig. 8d), that is, during 13 min in the temperature range −5.5° to −9°C. Supersaturation generation is higher than its absorption by the drops and crystals until 37 min; LWC grows and reaches a maximum of 2.2 g m^{-3} (versus 1.8–2.0 in HR90 at this stage); after that time absorption begins to prevail, the drops partially evaporate, LWC decreases to 1.3 g m^{-3} by 1 h (Fig. 8e), and IWC increases due to the Bergeron–Findeisen process (Fig. 8f). All of these characteristics (crystal concentrations and nucleation rates at this temperature range of −5° to −10°C, droplet concentration, and LWC) along with their temporal evolution are similar to those observed by HR90.

The effect of variations of the vertical velocity and α is as follows. Under the same initial conditions and different w, the general picture is similar but the maxima $N_c = 436$ L^{-1} with $w = 50$ cm s^{-1} and 1700 L^{-1} with $w = 1$ m s^{-1}; the cloud is mixed phase in the former case and fully glaciates in the last case by 1 h. To study the sensitivity to the surface fraction of active sites α, we performed several runs with the same parameters but $\alpha = 0$. Rapid glaciation in these runs began later, at temperatures lower by 4°–6°C, and with higher final crystal concentrations up to 1–4 ($\times 10^4$) L^{-1}. So, the agreement of the runs with $\alpha = 0$ with HR90 is worse, indicating that the active sites of CCN could play an important role in their freezing and rapid crystal formation in cumulus described in HR90. These simulations show that the action of active site is that the CCN freezing begins earlier at warmer temperatures and ceases earlier at warmer T, leading to a decrease in the final crystal concentration relative to the case with $\alpha = 0$.

We used here the values of α from the range given by Fletcher (1969); a more detail test would require many more parcel runs and is beyond the scope of this paper. A review of numerous experimental studies of the three types of aerosol active sites (morphological, chemical and electrical) is given in PK97 (chapters 5, 9), along with the conclusion that little is still known about their properties. Their essential effect on CCN freezing indicates the necessity of detailed microscopic studies of the CCN surface properties after sampling in the chamber and field experiments.

Note that the high N_c ($> 10^4$ L^{-1}) obtained with $\alpha = 0$ at lower T are not unrealistic, such values have been

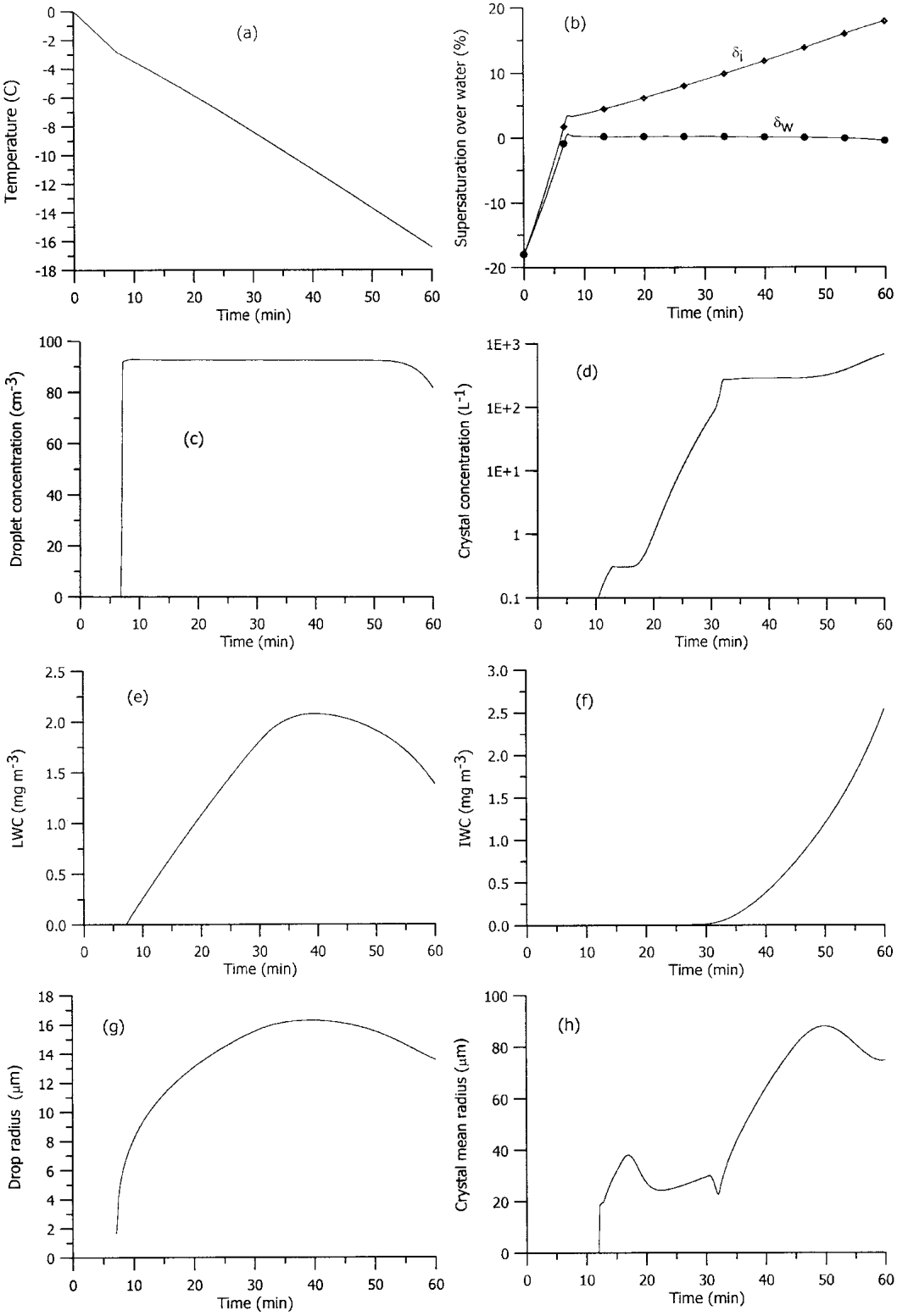

FIG. 8. Simulation of the rapid crystal nucleation in a small maritime Cu cloud similar to the case observed by Hobbs and Rangno (1990): evolution of the droplet and crystal microphysical properties with $w = 65$ cm s^{-1}, $\mathrm{RHW}_0 = 0.82$, $T_{c0} = 0°\mathrm{C}$, $m_{is} = 0.5$, $\alpha = 0.2 \times 10^{-5}$. (a) Temperature, °C; (b) supersaturations over water, δ_w, and ice, δ_i, %; (c) droplet concentration, cm^{-3}; (d) crystal concentration, L^{-1}; (e) liquid water content, g m^{-3}; (f) ice water content, g m^{-3}; (g) droplet mean radius, μm; (h) crystal mean radius, μm.

observed in Ac and Cu clouds even using older measurement techniques ($>10^4$ L^{-1}, Fig. 2–42 in PK97). Much higher values were recently observed in Arctic mixed clouds using newer devices that can count small crystals (from a few hundred to $> 4–7 \times 10^4$ L^{-1}; Lawson et al. 2001; Rangno and Hobbs 2001) and also in postconvective anvils (e.g., Knollenberg et al. 1993). These observations were made under conditions when ice multiplication mechanisms should not be effective.

An important result of our simulations with w = 0.5–1 m s^{-1} is that water supersaturation never exceeds 1% and is 0.15%–0.1% during the main crystal nucleation process in Fig. 8b, indicating that such high ice concentrations and nucleation rates as observed in HR90 and RH91 may occur in this theory without pockets of high water supersaturations, just via freezing of deliquescent mixed CCN at supersaturations typical of mixed clouds, near zero.

4. Comparison with homogeneous nucleation theory

During the last 15 years, the absence of a suitable heterogeneous nucleation theory has resulted in the development and refinement of models of homogeneous nucleation (a comprehensive analytical review is given in DeMott 2002). The different models of heterogeneous nucleation were compared in the Idealized Cirrus Model Comparison Project (ICMCP; Starr et al. 2000) and the CPMCP (Lin et al. 2002). All models used either homogeneous nucleation theory or various empirical parameterizations of heterogeneous nucleation. According to the theory presented here, both homogeneous and heterogeneous nucleation processes are similar except that the nucleation energy barrier is lower in the presence of an insoluble catalyzing substrate in the heterogeneous process. This concept is in agreement with the models employed in CPMCP for the heterogeneous freezing mode that also treats freezing of deliquescent mixed CCN as discussed in Part I and here.

For quantitative comparison of both the heterogeneous and homogeneous nucleation processes, we performed two series of experiments using the parcel model with either homogeneous freezing of the deliquescent CCN described in section 2C or heterogeneous freezing described in Part I under the conditions recommended for ICMCP and CPMCP; these two modes were switched on or off in the corresponding runs. The first series of simulations is for relatively "warm" cirrus at initial $T_0 = -40°C$ and the second series was for a cold cirrus at $T = -60°C$; pressure was p = 340 hPa, w = 4 cm s^{-1}, N_{CCN} = 200 cm^{-3}; contact parameter m_{is} = 0.5 for the heterogeneous case. The integration over the haze size spectrum was performed for the heterogeneous case, as described in Part I, and for the homogeneous case, the size spectrum recommended by CPMCP was used (Lin et al. 2002). Simulations for the warm cirrus are illustrated in Figs. 9 and 10. For convenience of comparison, the initial RHW_0 was chosen after several preliminary runs in such a way that both nucleation processes occurred at approximately the same time, 30 min after the start of the simulation. This required RHW_0 = 90% for homogeneous nucleation and only 78% for heterogeneous nucleation. The nucleation reaches a significant rate at RHW ≈ 97.6% for the homogeneous processes and at 83% for the heterogeneous processes (Fig. 9a). The critical radius is higher for heterogeneous nucleation because of lower humidity (Fig. 9b); however, the critical energy of heterogeneous nucleation is comparable and even a little smaller at t = 35 min than that for homogeneous nucleation (Fig. 9c). This is caused by the geometric factor $f(m_{is})$, which reduces the energy barrier for nucleation. The homogeneous $J_{hom} r_d^3$ and heterogeneous $J_{s,fr}(r_N, T)$ nucleation rates (s^{-1} per particle) calculated as an example for a haze particle of 0.13 μm (Fig. 9d) and polydisperse nucleation rates (Fig. 9e) are comparable although the maxima for heterogeneous nucleation is ~4 times higher due to this small difference in ΔF_{cr}. The final crystal concentrations are comparable: 118 L^{-1} in the heterogeneous case versus 56 L^{-1} in the homogeneous case (Fig. 9f).

Time evolutions of the heterogeneous versus homogeneous processes at –40°C are compared in Fig. 10. Both processes are similar in general (IWC, N_c, supersaturation relaxation time), although the lower water and ice supersaturations in the heterogeneous case lead to a smaller mean crystal radius and vapor excess. The percentage of condensed ice is higher with heterogeneous nucleation, so the efficiency of deposition is higher in this case. Crystal size spectra 30 min after the main nucleation impulse (Fig. 11) have smaller maxima but are broader in the homogeneous nucleation process since the difference in crystal ages is greater due to the longer nucleation time.

An additional comparison of the two ice nucleation modes is shown in Fig. 12 at T = –60°C. This time, both runs were started at the same RHW_0 = 75% in order to determine the difference in the two modes. As in the previous case, heterogeneous nucleation starts much earlier, at t = 28 min at RHW ≈ 80%, and homogeneous nucleation begins 16 min later, at t = 44 min, at RHW ≈ 88% (Figs. 12a,b). The impulse of nucleation in the heterogeneous case is again narrower in time (Δt = 5 min versus Δt = 9 min), with comparable maxima of the nucleation rate ($R_{m,het} = 2.2 \times 10^{-3}$ cm^{-3} s^{-1} versus $R_{m,hom} = 2.9 \times 10^{-3}$ cm^{-3} s^{-1}), and comparable N_c = 188 L^{-1} versus 171 L^{-1} for heterogeneous and homogeneous cases, respectively. The entire cirrus development proceeds similarly in both cases but is shifted ~18 min later in the homogeneous case. Crystal size spectra for both heterogeneous and homogeneous nucleation at $T = -60°C$ (Fig. 13) are also closer to each other than the spectra at warmer $T = -40°C$ (Fig. 11). Thus, the difference between the two ice nucle-

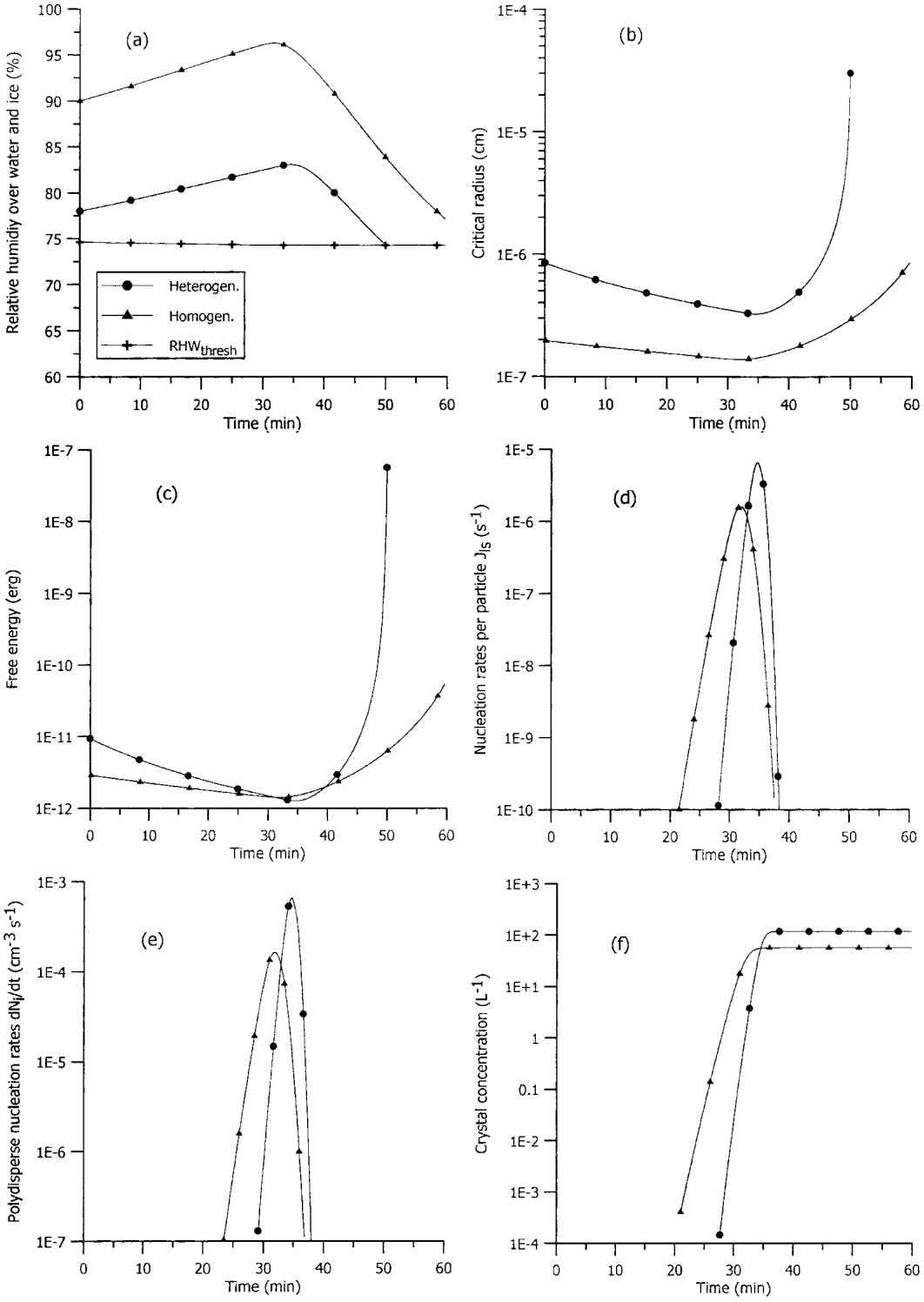

FIG. 9. Comparison of primary properties of heterogeneous (circles, m_{is} = 0.50, RHW_0 = 78%) and homogeneous (triangles, RHW_0 = 90%) nucleation processes at T_{0c} = −40°C, w = 4 cm s^{-1}, p_0 = 340 hPa. (a) Relative humidity over water and threshold humidity RHW_{th}, %, defined as $100S_{w,th}$ with use (3.9) in Part I; (b) ice germ critical radius r_{cr}, cm; (c) free energy ΔF_{cr}, erg; (d) homogeneous $J_{hom}r_d^3$ and heterogeneous $J_{f,ls}$ nucleation rates per particle, s^{-1}, calculated for a particle radius 0.13 μm with (2.1) in Part I and (2.18) here; (e) polydisperse nucleation rates, dN_f/dt, in cm^{-3} s^{-1}, defined by (4.5) in Part I; (f) crystal concentration, L^{-1}.

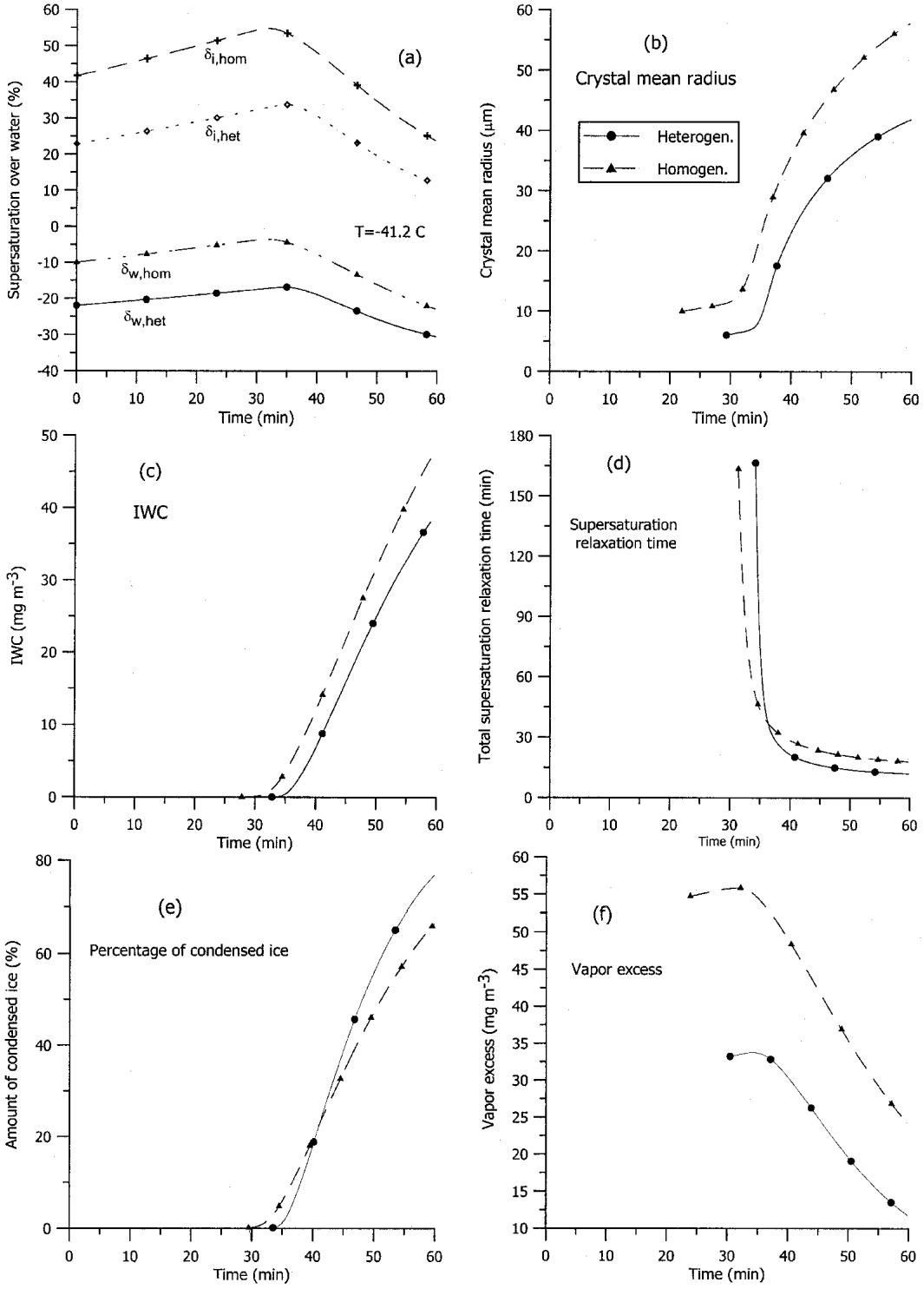

FIG. 10. Comparison of crystal microphysical properties with heterogeneous (circles) and homogeneous (triangles) nucleation processes at −40°C, $w = 4$ cm s^{-1}, and the other parameters as in Fig. 9. (a) Supersaturations over water, δ_w, and ice, δ_i, %; (b) crystal mean radius, μm; (c) ice water content, mg m^{-3}; (d) crystal supersaturation relaxation time, min; (e) relative amount of condensed ice, %; (f) vapor excess, mg m^{-3}.

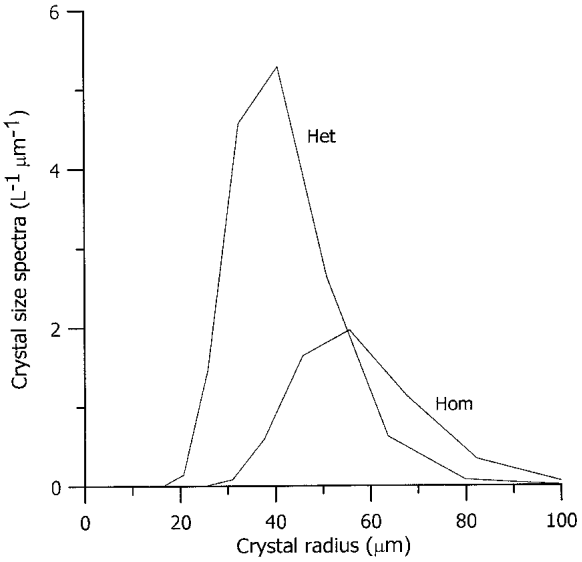

FIG. 11. Comparison of the crystal size spectra at $T = -40°C$ with homogeneous and heterogeneous nucleation after $t = 1$ h.

ation modes decreases with the lowering temperature. Note that crystal concentrations for both heterogeneous and homogeneous nucleation are quite comparable both at $-40°$ and $-60°C$, despite the fact that they were calculated with substantially different equations. This indicates that the heterogeneous theory can be used for the calculations of ice nucleation in cirrus.

Finally, we compare our results with the other four models from the CPMCP (Lin et al. 2002). Table 1 shows that our results for the warm homogeneous case (denoted Wh), $N_c = 0.056$ cm^{-3}, are in the middle of the range among the other models ($N_c = 0.0275$–0.081 cm^{-3}); the same is for the cold homogeneous case (Ch); ours is $N_c = 0.178$ cm^{-3} as compared to the others at $N_c = 0.138$–0.474 cm^{-3}. This agreement shows that our parcel model has sufficient accuracy and can be used for such simulations and the theory of homogeneous nucleation is sufficiently developed for quantitative descriptions. With heterogeneous nucleation, the range of the other four models is 0.0054–0.0183 cm^{-3} for Wa (warm all mode) and 0.0126–1.065 cm^{-3} for Ca (cold all mode, where mostly heterogeneous nucleation mode acts). Our heterogeneous nucleation results are comparable with the homogeneous nucleation method, 0.118 and 0.188 cm^{-3} for warm and cold cases since both processes are similar and proceed on the same CCN with comparable rates. However, heterogeneous nucleation requires lower humidity and starts earlier in a cooling air parcel.

5. Dependence of ice crystal concentration on temperature and supersaturation

To illustrate the general dependence $N_c(T)$, the final crystal concentrations obtained (when nucleation has ceased) in about 50 runs with $w = 1$, 2 and 5 cm s^{-1} are plotted in Fig. 14 versus the temperature when nucleation ceases along with the Fletcher (1962) parameterization

$$N_{\text{IN}} = N_0 \exp(\beta \Delta T), \tag{5.1}$$

where $N_0 = 10^{-5}$ L^{-1}, $\Delta T = T_0 - T$ is supercooling, and average $\beta = 0.6$. Figure 14 shows that the general tendency of the cloud phase state is transition from the liquid state at $T \geq -10°C$ to the mixed-phase state for $-12° < T < -18°C$, and to the crystalline state at $T_c < -20°C$. The results of the two runs with $m_{is} = 0.12$–0.32 and $w = 5$ cm s^{-1} (below Fletcher's curve) show that low crystal concentrations $N_c = 0.8$–3 L^{-1} formed with very small m_{is} do not allow complete glaciation of the cloud, and the liquid phase exists at temperatures as low as $-21°$ to $-26°C$. The same result was obtained with lower aerosol concentration (down to 50 cm^{-3}, not shown). Thus observation of mixed clouds at temperatures below $-20°C$, for example, arctic clouds in the Surface Heat Budget of the Arctic–First International Satellite Cloud Climatology Project (ISCCP) Regional Experiment (SHEBA–FIRE) experiment (Curry et al. 2000; Uttal et al. 2002) and strongly supercooled mixed altocumulus (Heymsfield et al. 1991) may be caused by the specific chemical composition of CCN that has an insoluble fraction with low contact parameter or by low CCN concentration.

Under relatively warm conditions ($T \geq -10°C$) and in weak updrafts ($w = 1$–2 cm s^{-1}), the cloud is almost entirely liquid for $m_{is} = 0.5$–0.55. Ice crystals could probably form in this temperature range with values of $S_w \sim 1.03$–1.05 (see Part I), but do not form here since the growing droplets do not allow supersaturations higher than ~0.1%–0.2%, which is insufficient for ice nucleation at these temperatures and contact parameters. At slightly higher values of $m_{is} = 0.6$–0.65 and in the presence of a small fraction of active sites, $\alpha = 2 \times 10^{-5}$, the probability of ice nucleation increases. These simulations and Fletcher's parameterization both show increasing N_c with decreasing T. However, the simulated curves are characterized by the two different slopes: the simulated slope is greater (and close to the slope of Fletcher's curve) at warmer $T > -20°C$, where mixed clouds form at $\delta_w > 0$ (marked in red), and the simulated slope becomes much smaller than Fletcher's at $T < -20°C$, where mostly crystalline clouds form at $\delta_w < 0$ (marked in blue). It is interesting to note that, although the dynamics in these simple parcel simulations is different from that in the continuous flow chambers, simulated values of N_c at $-10°C > T > -20°C$ are comparable to the range of those measured in chambers (e.g., Rogers 1982, 1994; Al-Naimi and Saunders 1985; Meyers et al. 1992). The simulated values of N_c are greater than Fletcher's parameterization at $T > -25°C$ but smaller at colder T. For a more detailed comparison with chamber experiments, this theory of

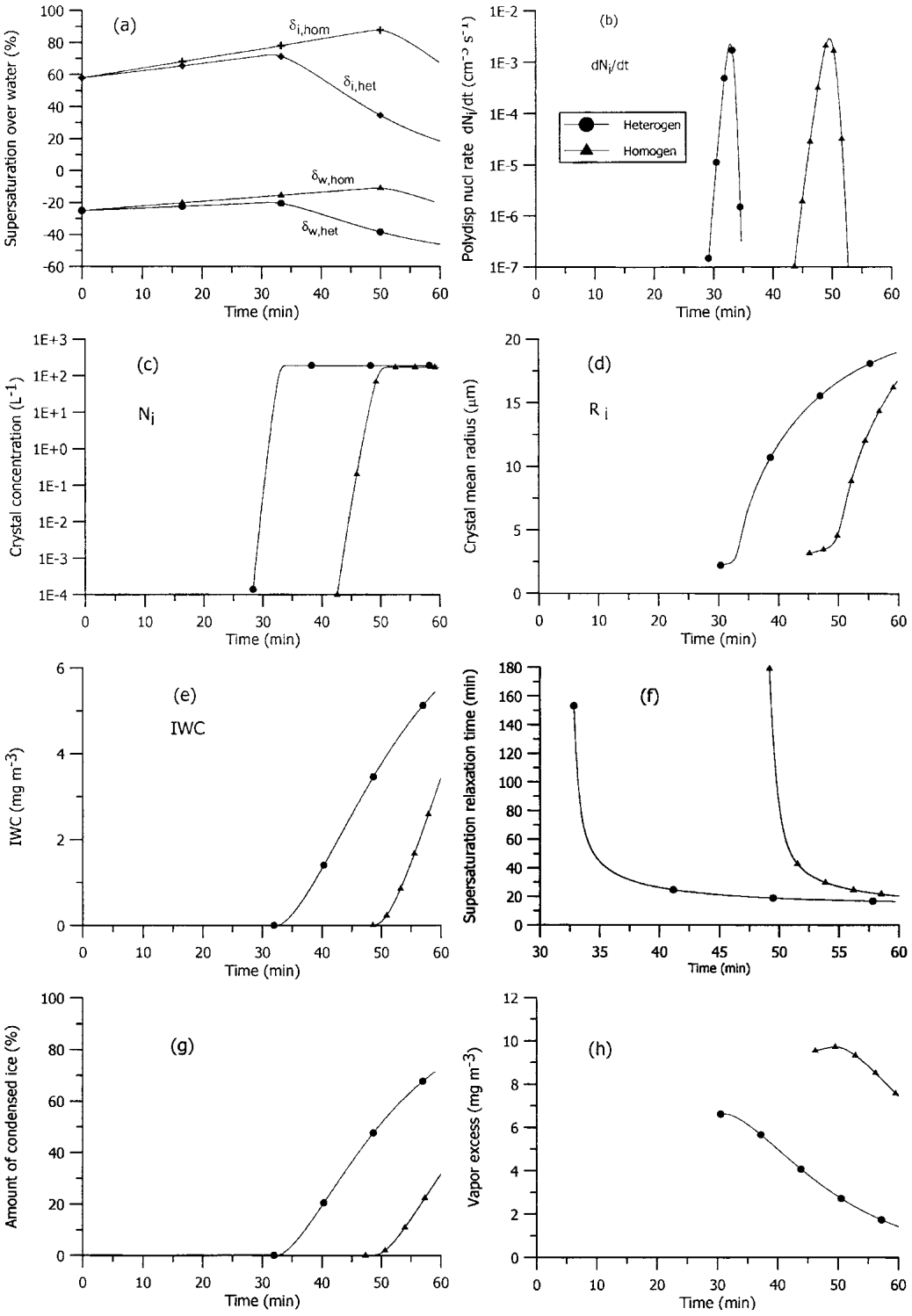

FIG. 12. Comparison of crystal microphysical properties with heterogeneous (circles) and homogeneous (triangles) nucleation processes at −60°C, w = 4 cm s^{-1}, RHW$_0$ = 75%. (a) Supersaturations over water δ_w and ice δ_i, %; (b) polydisperse nucleation rates, dN_{fr}/dt, in cm^{-3} s^{-1}, defined by (4.5) in Part I; (c) crystal concentration, L^{-1}; (d) crystal mean radius, μm; (e) ice water content, mg m^{-3}; (f) crystal supersaturation relaxation time, min; (g) relative amount of condensed ice, %; (h) vapor excess, mg m^{-3}.

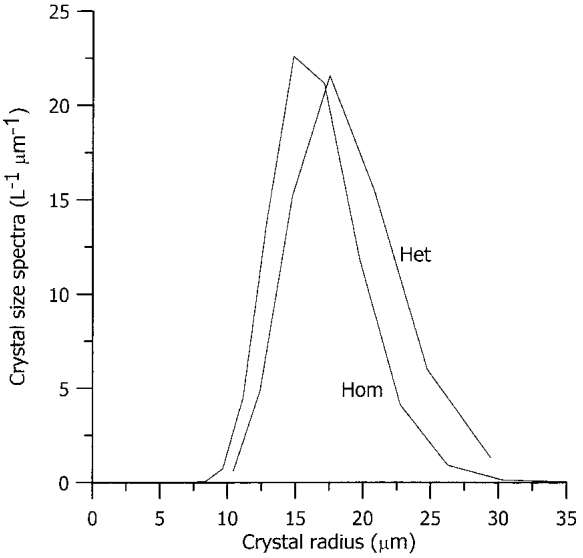

FIG. 13. Comparison of the crystal size spectra at $T = -60°C$ with homogeneous and heterogeneous nucleation after $t = 1$ h.

heterogeneous nucleation could be tested in a 2D model that simulates a vertical plane in a chamber.

Fletcher's parameterization was based on data available by the end of the 1950s and was obtained for temperatures mostly above −25°C. Its extrapolation down to very low temperatures produces very high values of N_c, which forced modelers to reject use of heterogeneous nucleation for cold cirrus and altostratus and invoke homogeneous nucleation for these clouds as the main nucleation mode or introduce various modifications to Fletcher's parameterization for cold T (e.g., Sassen and Dodd 1988, 1989; Heymsfield and Sabin 1989; DeMott et al. 1994; Jensen et al. 1994, 1996; Khvorostyanov and Sassen 1998b,c, 2002; Spice et al. 1999; Gu and Liou 2000; Lin et al. 2002; Kärcher and Lohmann 2002). The theory presented here is in accord with numerous observations in recent decades (e.g., Meyers et al. 1992, Fig. 2), and gives reasonable values of N_c at very cold temperatures in agreement with measurements in cirrus (e.g., Gayet et al. 1996; Chen et al. 1998; Rogers et al. 1998; Heymsfield and McFarquhar 2002; Lawson et al. 2001) and with the parameterization of heterogeneous nucleation freezing of solution drops developed by DeMott et al. (1998). Hence this theory of heterogeneous ice crystal nucleation can be used for simulation of cold altostratus, altocumulus, and cirrus clouds, serving as an alternative for homogeneous nucleation. A comparison of the runs performed at colder temperatures (below −20°C) showed that N_c increases by a factor ~3 when w increases from 1 to 2 cm s^{-1} and by ~4 when w increases from 2 to 5 cm s^{-1}, indicating the nonlinear dependence of N_c on w similar to the parameterization found for homogeneous nucleation in Kärcher and Lohmann (2002).

TABLE 1. Comparison of the crystal concentrations, cm^{-3}, calculated here using this parcel model with $w = 4$ cm s^{-1}, heterogeneous nucleation theory (KC00) and homogeneous theory (KS98), with the results from the parcel intercomparison project CPMCP (Lin et al. 2002). Capital letters indicate the author of the model as L: Lin, S: Sassen, X: Xiahong Liu, and D: DeMott. "W" means warm case (−40°C), "C" means cold (−60°C), "h" means homogeneous nucleation, and "a" means "all modes" (actually heterogeneous case).

	Model				
Case	KC00 and KS98	L	S	X	D
Ca (het)	0.188	0.0126	1.0655	—	0.4027
Ch (hom)	0.178	0.1380	0.1640	0.281	0.4740
Wa (het)	0.118	0.0054	0.0183	—	0.0064
Wh (hom)	0.056	0.0286	0.0275	0.044	0.0810

A distinguishing feature of pristine N_c found in many experiments and discussed in Part I is its dependence on ice or water supersaturation (e.g., Huffman 1973; Rogers 1982, 1994; Hussain and Saunders 1984; Al Naimi and Saunders 1985; Berezinsky and Stepanov 1986; Rogers et al. 2001). These studies found that a power law described this dependence as

$$N_c(\delta_i) = C_i \delta_i^b \tag{5.2}$$

with values $3 < b < 8$, while an exponential parameterization was suggested by Meyers et al. (1992). Figure 15 illustrates the ice supersaturation dependence $N_c(\delta_i)$ calculated using the parcel model. Each solid symbol on the curves corresponds to a final N_c (after nucleation ceased) in a single run of the parcel model for 1–3 hours with $w = 1$, 2, and 5 cm s^{-1} plotted against the maximum value of δ_i during the run (reached usually near maximum N_c). The contact parameter m_{is} = const = 0.52 along the lines with the other values shown near the points.

Figure 15 shows the main features of the simulated $N_c(\delta_i)$: 1) increasing N_c with increasing δ_i and 2) marked decrease of the slopes $dN_c(\delta_i)/d\delta_i$ at $\delta_i > 15\%$–20%, that is, some sort of "saturation" at higher δ_i. The latter feature, convex dependence $N_c(\delta_i)$ with decreasing slopes, is similar to the measured water supersaturation dependence in the drop nucleation power law (e.g., Yum and Hudson 2001) and to the ice supersaturation dependence for ice nucleation described by (5.2) and measured at constant temperatures (e.g., Rogers 1982; Al-Naimi and Saunders 1985; Berezinsky and Stepanov 1986; Meyers et al. 1992). This functional similarity is caused by the analogous negative feedback with respect to supersaturation of both drop and crystal nucleation, although the latter is much stronger as discussed above. Note again, a more detailed comparison with the laboratory data can be done using a more sophisticated model closer to the chamber conditions.

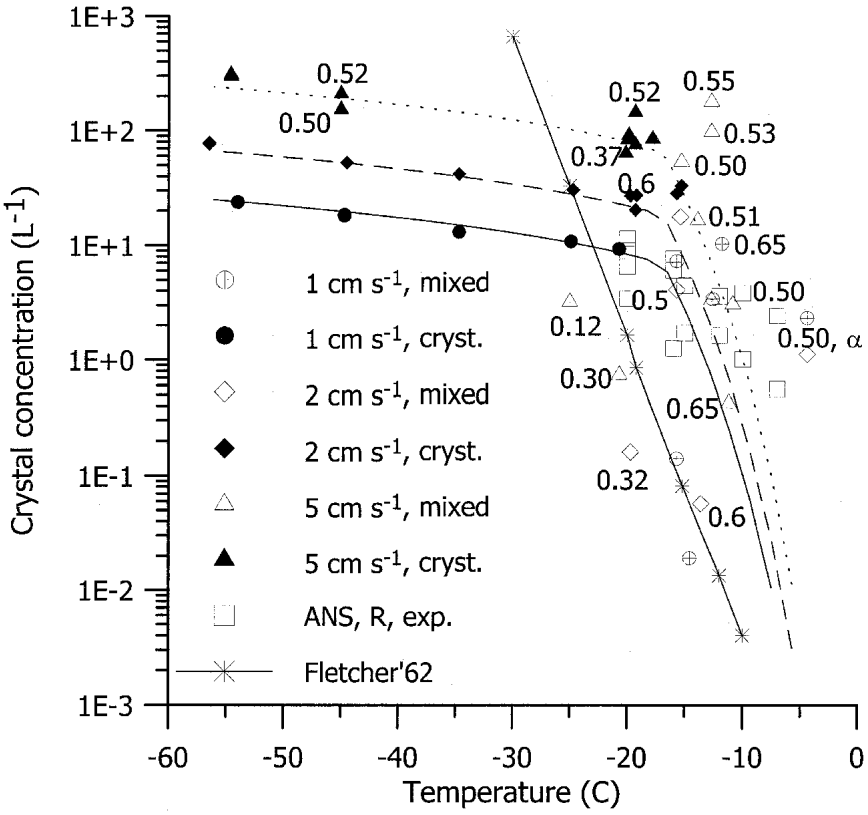

FIG. 14. Temperature dependence of the crystal concentrations N_c calculated with $w = 1$ (circles), 2 (diamonds), and 5 cm s^{-1} (triangles). Each symbol corresponds to a final N_i after a single run of the parcel model. The values of the contact parameter $m_{is} = 0.52 = \text{const}$ along the continuous lines, and other values of m_{is} are shown near the points; the symbol "α" denotes the runs with $\alpha = 2 \times 10^{-5}$. Open symbols denote CCN freezing at $\delta_w > 0$ in the presence of drops (mixed cloud, mostly at $T_c > -20$°C, although the mixed phase can be below −20°C with lower m_{is}), and solid symbols denote ice nucleation at $\delta_w < 0$ (crystalline cloud). Open squares denote laboratory data from Al Naimi and Saunders (1985) and Rogers (1982). The lines are fits to the data with the corresponding w as $N_c(T,w) = C_g(T_{c0} - T_c)^{C_T} w^{C_w}$, with $C_w = 1.41$, and two sets of other constants: $T_{c0} = 0$°C, $C_g = 0.4 \times 10^{-8}$, $C_T = 8.0$, for $T_c > -15$°C; and $C_g = 0.535$, $C_T = 1.05$ for $T_c = < -15$°C. These fits might be used as a simple parameterization of the average data in cloud models and GCMs.

6. Summary and conclusions

This theory provides a quantitative description of heterogeneous crystal nucleation by freezing of mixed CCN that is in agreement with observations by Hobbs and Rangno (1990) and Rangno and Hobbs (1991) of rapid crystal nucleation in maritime cumulus and with the parcel model of DeMott et al. (1998) based on the recent measurements of the IN with large soluble fractions (Chen et al. 1998; Rogers et al. 1998, 2001). The theory gives crystal concentrations and nucleation rates that depend on both temperature and water (or ice) saturation ratio and provides the foundation for parameterization of ice nucleation in cloud-scale and large-scale models. The modeled T dependence of N_c is similar to, yet different from, Fletcher's (1962) parameterization. The similarity is associated with increasing N_c for decreasing T. The difference is that this theory yields greater N_c at $T > -25$°C and smaller N_c at lower T, in agreement with recent measurements of N_c (e.g., Meyers et al. 1992; PK97; Rogers et al. 2001). The theory produces reasonable N_c for all T to below −60°C and can be used for simulation of ice formation in all cloud types from stratocumulus to cirrus.

Our theory shows that deliquescence-freezing nucleation may occur under conditions of water supersaturations in the presence of drops in clouds (primarily at T from −5° to −20°C) as well as subsaturation in clear air (diamond dust or cirrus, mostly at $T < -20$°C). Our parcel model simulations show that this theory reproduces the observed dependence of N_c on water and ice supersaturations: 1) crystal concentration $N_c(\delta_i)$ is a smooth function at transitions between water super- and subsaturations similar to that observed in the chambers (power or exponential law); 2) increasing N_c with growing δ_i; 3) displacement of the curves to the

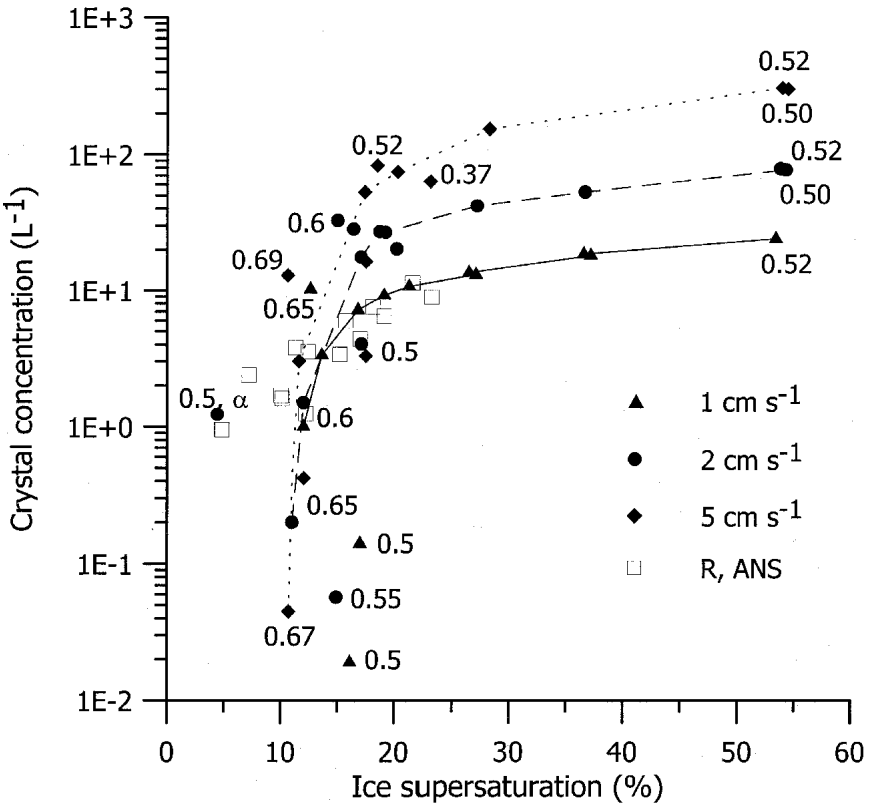

FIG. 15. The ice supersaturation dependence of the crystal concentration $N_c(\delta_i)$. Each symbol corresponds to a final N_i after a single run of the parcel model. Triangles, circles, and diamonds denote simulations with vertical velocity w = 1, 2, and 5 cm s^{-1}. The contact parameter m_{is} = 0.52 along the fitting lines and is indicated near the points where it is different; the symbol α denotes the runs with $\alpha = 2 \times 10^{-5}$. Open squares denote laboratory data from Rogers (1982) and Al Naimi and Saunders (1985).

higher δ_i at lower T; and 4) significant decrease of the slopes $dN_c(\delta_i)/d\delta_i$ at $\delta_i > 15\%$–20%. These features have been observed for more than three decades and have been parameterized individually by many authors cited previously in this paper.

We performed two series of runs of the parcel model with this ice nucleation scheme and vertical velocities w = 1–5 cm s^{-1} that may imitate ice nucleation in synoptic-scale updrafts and w = 0.5–1 m s^{-1}, which are typical of wave- or convective-type clouds. The values of N_c calculated at w = 1–5 cm s^{-1} and average m_{is} = 0.5 range from $\sim 10^{-2}$ to 10^2 L^{-1}, and are comparable to those measured in continuous flow diffusion chambers (e.g., Rogers 1982, 1994; Al-Naimi and Saunders 1985; Meyers et al 1992) and in field experiments in stratiform clouds (e.g., PK97). The concentrations simulated with a little higher m_{is} = 0.55–0.65 are substantially greater than typical IN concentrations in the chambers, reach a few tens to a few hundred per liter and are comparable to those measured recently by Rangno and Hobbs (2001) and Lawson et al. (2001) in Arctic stratiform clouds. The analysis in cited works showed that the Hallett–Mossop or other ice multiplication mechanisms could not operate in many cases, and an explanation of these high concentrations remained elusive. Based on our parcel runs, we can hypothesize that the CCN deliquescence-freezing mechanism could be responsible for these high N_c at least in some cases. Support for this hypothesis comes from the high (up to 65%) fraction of spheroidal crystals that could not be formed by splintering (Lawson et al. 2001) but could be diffusion-grown frozen CCN.

Numerical experiments showed that the nucleation rates increase substantially with increasing vertical velocity. Simulation with w = 0.5–1 m s^{-1} showed that N_c can reach 400–1700 L^{-1} due to CCN freezing in a mixed-phase cumulus cloud at warmer temperatures $-5°$ to $-10°$C so that the simulated cloud microphysical properties were very similar to those observed by Hobbs and Rangno (1990) and Rangno and Hobbs (1991) in marine cumulus. Their analysis showed that the ice multiplication mechanisms could not explain this rapid nucleation and they hypothesized that freezing of residual interstitial CCN may produce such high N_c and that high water supersaturations of 5%–10% may be required. Our work confirms both conceptually

and quantitatively the first point, but this unusually high supersaturation is not required.

A remarkable feature of heterogeneous drop nucleation on soluble and mixed CCN is its self-regulatory character with a negative feedback: when the rate of supersaturation absorption by the nucleated drops exceeds the rate of supersaturation production, then supersaturation begins to decrease and nucleation stops. Classical heterogeneous freezing theory did not predict the same behavior for crystals since the freezing mechanism did not have the negative feedback via supersaturation, as did the supersaturation power law for the drops. The theory by Fukuta and Schaller (1982) showed that such negative feedback may occur due to supersaturation dependence of the condensation on insoluble nuclei; however this feature was related to the insoluble aerosols and not to the natural mixed CCN, and has not been previously investigated in detail with a dynamical cloud model.

Our theory accompanied by the parcel simulations shows that a negative supersaturation feedback also exists for freezing of deliquescent mixed CCN: ice nucleation ceases as supersaturation begins to decrease despite continuing cooling. This negative feedback is analogous to the nucleation of cloud drops, but there is significant dissimilarity in kinetics of these processes. The major difference in these mechanisms is that drop formation is characterized by a rapid nucleation rate and slow diffusional growth rate, while ice crystal nucleation is characterized by slow nucleation rate and rapid diffusional growth rate. Thus in our model, only a tiny fraction of the same CCN that nucleate drops may nucleate crystals. So, it might not be the different concentrations of the aerosol particles (insufficient IN and abundant CCN) that determine the large difference in drop and crystal concentrations in the clouds, but rather the different mechanisms of their formation on similar populations of aerosol particles.

The third series of parcel runs for colder cirrus temperatures $\leq -40°C$ shows that both heterogeneous and homogeneous ice crystal nucleation may proceed at cold temperatures in similar ways: by deliquescence of CCN and formation and freezing of the haze particles. The difference between the two modes is that heterogeneous freezing of a solution occurs on the surface of its insoluble substrate that serves as a nucleation catalyst, while homogeneous freezing arises in the bulk solution without a foreign substance. At temperatures below $-40°C$, crystal concentrations are higher in the heterogeneous mode with $m_{is} = 0.5$, although the concentrations are comparable in both modes and N_c in the heterogeneous mode could be lower with smaller m_{is}. If both processes are allowed and both fully soluble and mixed aerosol particles are available, a noticeable difference in the required relative humidity (14% at $-40°C$ and 9% at $-60°C$) would prevent homogeneous nucleation since heterogeneous nucleation is initiated at lower values of relative humidity. This concept is in agreement with the general discussion in Detwiler (1989) and Sassen (1989) and simulations by DeMott et al. (1994), Jensen et al. (1994), Khvorostyanov and Sassen (1998b,c, 2002), Spice et al. 1999, Sassen and Benson (2000), Gu and Liou (2000), Starr et al. (2000), Gierens (2003), Lin et al. (2002), and DeMott (2002).

Alternatively, if only completely soluble CCN are present without any insoluble admixture, the homogeneous mode will dominate as was found by Sassen and Dodd (1988, 1989), Heymsfield and Sabin (1989), DeMott et al. (1994). The same situation occurs in this theory if the contact parameter m_{is} is too small to initiate heterogeneous nucleation. The clarifications provided here are 1) the same CCN may be involved in both homogeneous and heterogeneous processes, in close agreement with observations by DeMott et al (1998) and modeling results reported by Lin et al. (2002), and 2) a quantitative method is suggested for evaluation of heterogeneous freezing of the mixed CCN at both water sub- and supersaturations.

Whether heterogeneous or homogeneous ice nucleation dominates at low temperatures depends on the nature and physio-chemical properties of the local CCN. The heterogeneous mode may prevail in regions with deep convection or strong advection of aerosols that bring large amounts of minerals and other insoluble materials into the middle and upper troposphere with subsequent formation of mixed CCN. Such a situation was observed during the recent Cirrus Regional Study of Tropical Anvils and Cirrus Layers–Florida Area Cirrus Experiment (CRYSTAL FACE) experiment in July 2002 over Florida (DeMott et al. 2003; Sassen et al. 2003). In oceanic regions that are deficient in insoluble substances, cirrus may be generated primarily via the homogeneous mode, although the long-range transport of wind-blown mineral dust in the atmosphere is increasingly being observed in remote oceanic regions.

Further verification and application of this theory requires precise measurements of the insoluble fraction inside CCN: size distributions and their physio–chemical properties (contact parameter, surface tension, latent heat, activation energy, critical radius and energy, especially at low temperatures). Since the parcel model used here is a simplified one, this ice nucleation theory can be tested further by incorporation into more complete multidimensional numerical models with fine resolution. This scheme was included into a 3D cloud-resolving model with explicit bin microphysics to simulate a cloud system over an Arctic polynya (Khvorostyanov et al. 2003) and is being used in the development of a double-moment microphysics parameterization (Morrison et al. 2005). Both of these papers showed that this heterogeneous nucleation theory allows reproduction of observed ice crystal concentrations, cloud phase structure, and life cycle in multidimensional models. The parameterization is also being incorporated into the Canadian Northern Aerosol Re-

gional Climate Model (E. Girard 2003, personal communication). The FORTRAN subroutines for tests in another models are available from the authors.

These results have significant implications for the parameterization of ice nucleation in cloud and climate models. Since the lifetime of a quasi-isolated lifting cloud parcel where ice nucleation occurs can be shorter than the complete nucleation cycle, this implies that the most relevant parameter is not the "final" crystal concentration, which may never be reached in a updraft, but rather the nucleation rates. Given these rates, a cloud regulates ice production by the magnitude and duration of the vertical velocities via supersaturation and mixing among the parcels. To develop a parameterization of ice nucleation for large-scale models, the kinetic ice nucleation process should be incorporated into multidimensional models with fine spatial resolution [e.g., large eddy simulation and cloud resolving models] that explicitly include entrainment, precipitation, and updraft fluctuations. Improvement of the ice nucleation schemes in cloud and climate models is one of the tasks of the Global Energy and Water Cycle Experiment (GEWEX) Cloud System Study (e.g., Randall et al. 2003).

Acknowledgments. This research has been supported by grants from the Department of Energy (DOE) Atmospheric Radiation Program and NASA CRYSTAL–FACE. We would like to thank the three anonymous reviewers for reading the manuscript and providing useful remarks; P. DeMott for providing the data from the continuous flow chambers and useful discussions; and R.-F. Lin for providing the data on the parcel models comparison. The assistance of Jody Norman in preparation of the manuscript is gratefully acknowledged.

APPENDIX

List of Symbols

B	Kelvin curvature parameter
b	The index of the power-law parameterization of $N_c(\delta_i)$, Eq. (4.2)
c_1, c_2	The coefficients defined in (2.12b) and (2.13b)
c_p	The specific heat capacity at constant pressure
D	The water vapor diffusivity coefficient
E_{dr}	"Condensation efficiency" of CCN in producing the droplets
$E_{\rm cr}$	"Freezing efficiency" of deliquescent CCN in producing the crystals
$\Delta F_{\rm act}$	The activation energy for diffusion across the liquid–ice boundary
$\Delta F_{\rm cr}$	The critical energy of heterogeneous nucleation of an ice germ
$\Delta F_{g,\rm hom}$	The critical energy of homogeneous nucleation of an ice germ
$f(m_{is}, x)$	The geometrical factor in equation for $\Delta F_{\rm cr}$ defined in Part I
$f_c(r_c)$, $f_d(r_d)$	The size distribution functions of the crystals and droplets
$f_a(r_N)$	The size distribution function of the insoluble fraction of the CCN
g	The acceleration of gravity
$I_{\rm dep}$ and $I_{\rm con}$	The deposition vapor flux to the crystals and condensation flux to the droplets
$J_{\rm hom}$	The homogeneous nucleation rate
$J_{s,\rm fr}$	The heterogeneous nucleation rate
L_e, L_s	The specific latent heats of evaporation and sublimation
M_w and M_a	The molecular weights for water and dry air
m_{is}	The contact parameter or wettability
N_0	The number of molecules in contact with a unit area of ice
$N_{\rm CCN}$, N_a	Concentration of the CCN
N_c, N_d	The crystal and droplet number concentrations
$N_{\rm IN}$	The number concentration of IN
$n(\delta_{w0})$	CCN activity spectrum
p	Pressure
p_0	Initial pressure in a parcel run
R, R_a, R_v,	Universal gas constant and specific gas constants for the dry air and for water vapor
$R_M = N_c/N_{\rm IN}$	The ice enhancement factor
$R_{\rm fr}$	Heterogeneous freezing nucleation rate
$R_{m,\rm het}$, $R_{m,\rm hom}$	Maxima of the heterogeneous and homogeneous nucleation rates
$\rm RHW_0$	The initial relative humidity over water in a parcel run
r_b	The boundary radius of interstitial CCN defined after (2.15)
r_c, r_d	The crystal and droplet radii
$\bar{r}_c$,$\bar{r}_d$	The crystal and droplet mean radii
$\dot{r}_c$,$\dot{r}_d$	Growth rates of the crystal and droplet radii
$r_{\rm cr}$	The ice germ critical radius
r_m	The modal radius of the size spectrum of insoluble fraction
r_N	Radius of the insoluble fraction of the CCN
T_{0c}	The initial temperature in a parcel run
T	Temperature in kelvin
t, Δt	Time, time step
w	The vertical velocity
α	The surface fraction of active sites
α_d, α_c	The deposition and condensation coefficients
$\beta_{\rm dep}$, $\beta_{\rm con}$	Kinetic coefficients defined in (2.9a,b)
δ_w, δ_i	Relative supersaturations over water and ice
δ_{wm}, δ_{im}	Maximum supersaturations over water and over ice

$\delta_{w,\mathrm{th}}$	The threshold supersaturation over water
ε	The misfit strain
Γ_1, Γ_2, Γ_{12}	Psychrometric corrections defined in (2.7)
ρ_a, ρ_v	The air and water vapor densities
ρ_i, ρ_w	Densities of ice and water
ρ_{ws}, ρ_{is}	Saturated vapor densities over water and ice
σ	Dispersion of the size spectrum of insoluble fraction
σ_{abs}	The absolute dispersion of the crystal size spectra
τ_{fc}, τ_{fd}	The supersaturation relaxation times for the crystals and droplets
ψ_{fc}, ψ_{fd}	The source terms on the kinetic equation defined in (2.15)–(2.17)

REFERENCES

Al-Naimi, R., and C. P. R. Saunders, 1985: Measurements of natural deposition and condensation-freezing ice nuclei with a continuous flow chamber. *Atmos. Environ.,* **19,** 1871–1882.

Berezinsky, N. A., and G. V. Stepanov, 1986: Dependence of natural ice-forming nuclei concentration of different size on the temperature and supersaturation. *Izv. Acad. Sci. USSR, Atmos. Oceanic Phys.,* **22,** 722–727.

Buikov, M. V., 1961: Kinetics of distillation in a polydisperse fog. *Izv. Acad. Sci. USSR. Ser. Geophys.,* **7,** 1058–1065.

——, 1963: A method of the kinetic equations in the theory of clouds. *Proc. All-Union Meteor. Conf.*, Leningrad, USSR, State Committee for Hydrometeorology USSR, No. 5, 122–128.

Chen, Y., S. M. Kreidenweis, L. M. McInnes, D. C. Rogers, and P. J. DeMott, 1998: Single particle analyses of ice nucleating aerosols in the upper troposphere and lower stratosphere. *Geophys. Res. Lett.,* **25,** 1391–1394.

Cotton, W. R., G. J. Tripoli, R. M. Rauber, and E. A. Mulvihill, 1986: Numerical simulation of the effects of varying ice nucleation rates and aggregation process on orographic snowfall. *J. Climate Appl. Meteor.,* **25,** 1658–1680.

Curry, J. A., F. G. Meyer, L. F. Radke, C. A. Brock, and E. E. Ebert, 1990: Occurrence and characteristics of lower tropospheric ice crystals in the Arctic. *Int. J. Climatol.,* **10,** 749–764.

——, and Coauthors, 2000: FIRE Arctic Clouds Experiment. *Bull. Amer. Meteor. Soc.,* **81,** 5–30.

DeMott, P. J., 2002: Laboratory studies of cirrus cloud processes. *Cirrus,* D. Lynch et al., Eds., Oxford University Press, 102–135.

——, M. P. Meyers, and W. R. Cotton, 1994: Parameterization and impact of ice initiation processes relevant to numerical model simulation of cirrus clouds. *J. Atmos. Sci.,* **51,** 77–90.

——, D. C. Rogers, S. M. Kreidenweis, Y. Chen, C. H. Twohy, D. Baumgardner, A. J. Heymsfield, and K. R. Chan, 1998: The role of heterogeneous freezing nucleation in upper tropospheric clouds: Inferences from SUCCESS. *Geophys. Res. Lett.,* **25,** 1387–1390.

——, K. Sassen, M. R. Poellot, D. Baumgardner, D. C. Rogers, S. Brooks, A. J. Prenni, and S. Kreidenweis, 2003: African dust aerosols as atmospheric ice nuclei. *Geophys. Res. Lett.,* **30,** 1732, doi:10.1029/2003GL017410.

Detwiler, A., 1989: Comments on "Homogeneous nucleation rate for highly supercooled cirrus cloud droplets." *J. Atmos. Sci.,* **46,** 2344–2345.

Fletcher, N. H., 1962: *The Physics of Rainclouds.* Cambridge University Press, 390 pp.

——, 1969: Active sites and ice crystal nucleation. *J. Atmos. Sci.,* **26,** 1266–1278.

Fukuta, N., and R. C. Schaller, 1982: Ice nucleation by aerosol particles: Theory of condensation-freezing nucleation. *J. Atmos. Sci.,* **39,** 648–655.

Gayet, J.-F., G. Febvre, G. Brogniez, H. Chepfer, W. Regner, and P. Wendling, 1996: Microphysical and optical properties of cirrus and contrails: Cloud field study on 13 October 1989. *J. Atmos. Sci.,* **53,** 126–138.

Gierens, K., 2003: On the transition between heterogeneous and homogeneous freezing. *Atmos. Chem. Phys.,* **3,** 437–446.

Gu, Y., and K. N. Liou, 2000: Interactions of radiation, microphysics, and turbulence in the evolution of cirrus clouds. *J. Atmos. Sci.,* **57,** 2463–2479.

Hallett, J., and S. C. Mossop, 1974: Production of secondary ice particles during the riming process. *Nature,* **249,** 26–28.

Heymsfield, A. J., and R. M. Sabin, 1989: Cirrus crystal nucleation by homogeneous freezing of solution droplets. *J. Atmos. Sci.,* **46,** 2252–2264.

——, and G. M. McFarquhar, 2002: Mid-latitude and tropical cirrus. *Cirrus,* D. Lynch et al., Eds., Oxford University Press, 78–101.

——, L. M. Miloshevich, A. Slingo, K. Sassen, and D. O'C. Starr, 1991: An observational and theoretical study of highly supercooled altocumulus. *J. Atmos. Sci.,* **48,** 923–945.

Hobbs, P. V., 1969: Ice multiplication in clouds. *J. Atmos. Sci.,* **26,** 315–318.

——, and A. L. Rangno, 1990: Rapid development of high ice particle concentrations in small polar maritime cumuliform cloud. *J. Atmos. Sci.,* **47,** 2710–2722.

——, M. K. Politovich, and L. F. Radke, 1980: The structures of summer convective clouds in eastern Montana. I: Natural clouds. *J. Appl. Meteor.,* **19,** 645–663.

Huffman, P. J., 1973: Supersaturation spectra of AgI and natural ice nuclei. *J. Appl. Meteor.,* **12,** 1080–1082.

Hussain, K., and C. P. R. Saunders, 1984: Ice nucleus measurement with a continuous flow chamber. *Quart. J. Roy. Meteor. Soc.,* **110,** 75–84.

Jeffery, C. A., and P. H. Austin, 1997: Homogeneous nucleation of supercooled water: Results from a new equation of state. *J. Geophys. Res.,* **102** (D21), 25 269–25 279.

Jensen, E. J., O. B. Toon, D. L. Westphal, S. Kinne, and A. J. Heymsfield, 1994: Microphysical modeling of cirrus, 1. Comparison with 1986 FIRE IFO measurements. *J. Geophys. Res.,* **99,** 10 421–10 442.

——, ——, H. B. Selkirk, J. D. Spinhirne, and M. R. Schoeberl, 1996: On the formation and persistence of subvisual cirrus near the tropical tropopause. *J. Geophys. Res.,* **101,** 21 361–21 375.

Kärcher, B., and U. Lohmann, 2002: A parameterization of cirrus cloud formation: Homogeneous freezing of supercooled aerosols. *J. Geophys. Res.,* **107,** 4010, doi:10.1029/2001JD000470.

——, T. Peter, U. M. Biermann, and U. Schumann, 1996: The initial composition of jet condensation trails. *J. Atmos. Sci.,* **53,** 3066–3083.

Khvorostyanov, V. I., 1995: Mesoscale processes of cloud formation, cloud–radiation interaction and their modelling with explicit cloud microphysics. *Atmos. Res.,* **39,** 1–67.

——, and K. Sassen, 1998a: Toward the theory of homogeneous nucleation and its parameterization for cloud models. *Geophys. Res. Lett.,* **25,** 3155–3158.

——, and ——, 1998b: Cirrus cloud simulation using explicit microphysics and radiation. Part I: Model description. *J. Atmos. Sci.,* **55,** 1808–1821.

——, and ——, 1998c: Cirrus cloud simulation using explicit microphysics and radiation. Part II: Microphysics, vapor and ice mass budgets, and optical and radiative properties. *J. Atmos. Sci.,* **55,** 1822–1845.

——, and J. A. Curry, 1999a: A simple analytical model of aerosol

properties with account for hygroscopic growth. Part I: Equilibrium size spectra and CCN activity spectra. *J. Geophys. Res.,* **104** (D2), 2175–2184.
——, and ——, 1999b: Toward the theory of stochastic condensation in clouds. Part I: A general kinetic equation. *J. Atmos. Sci.,* **56,** 3985–3996.
——, and ——, 1999c: Toward the theory of stochastic condensation in clouds. Part II: Analytical solutions of gamma distribution type. *J. Atmos. Sci.,* **56,** 3997–4013.
——, and ——, 2000: A new theory of heterogeneous nucleation for application in cloud and climate models. *Geophys. Res. Lett.,* **27,** 4081–4084.
——, and K. Sassen, 2002: Microphysical processes in cirrus and their impact on radiation: A mesoscale modeling perspective. *Cirrus,* D. Lynch et al., Eds., Oxford University Press, 397–432.
——, and J. A. Curry, 2004: The theory of ice nucleation by heterogeneous freezing of deliquescent mixed CCN. Part I: Critical radius, energy, and nucleation rate. *J. Atmos. Sci.,* **61,** 2676–2691.
——, ——, J. O. Pinto, M. Shupe, B. Baker, and K. Sassen, 2001: Modeling with explicit spectral water and ice microphysics of a two-layer cloud system of altostratus and cirrus observed during the FIRE Arctic Clouds Experiment. *J. Geophys. Res.,* **106,** 15 099–15 112.
——, ——, I. Gultepe, and K. Strawbridge, 2003: A springtime cloud over the Beaufort Sea polynya: 3D simulation with explicit spectral microphysics and comparison with observations. *J. Geophys. Res.,* **108,** 4296, doi:10.1029/2001JD001489.
Knollenberg, R. G., K. Kelly, and J. C. Wilson, 1993: Measurements of high number densities of ice crystals in the tops of tropical cumulonimbus. *J. Geophys. Res.,* **98,** 8639–8664.
Lawson, P. R., B. A. Baker, C. G. Schmitt, and T. L. Jensen, 2001: An overview of microphysical properties of Arctic clouds observed in May and July 1998 during FIRE ACE. *J. Geophys. Res.,* **106** (D14), 14 989–15 014.
Lin, R.-F., D. O'C. Starr, P. J. DeMott, R. Cotton, K. Sassen, E. Jensen, B. Kärcher, and X. Liu, 2002: Cirrus parcel model comparison project. Phase 1: The critical components to simulate cirrus initiation explicitly. *J. Atmos. Sci.,* **59,** 2305–2329.
Meyers, M. P., P. J. DeMott, and W. R. Cotton, 1992: New primary ice-nucleation parameterizations in an explicit cloud model. *J. Appl. Meteor.,* **31,** 708–721.
Morrison, H., J. A. Curry, and V. I. Khvorostyanov, 2005: A new double-moment microphysics parameterization for application in cloud and climate models. Part I: Description. *J. Atmos. Sci.,* in press.
Ohtake, T., K. Jayaweera, and K. I. Sakurai, 1982: Observation of ice crystal formation in lower Arctic atmosphere. *J. Atmos. Sci.,* **39,** 2898–2904.
Pinto, J. O., J. A. Curry, and J. M. Intrieri, 2001: Cloud–aerosol interactions during autumn over Beaufort Sea. *J. Geophys. Res.,* **106,** 15 077–15 097.
Pruppacher, H. R., and J. D. Klett, 1997: *Microphysics of Clouds and Precipitation.* 2d ed. Kluwer, 997 pp.
Randall, D., and Coauthors, 2003: Confronting models with data: The GEWEX Cloud System Study. *Bull. Amer. Meteor. Soc.,* **84,** 455–469.
Rangno, A. L., and P. V. Hobbs, 1991: Ice particle concentrations and precipitation development in small polar maritime cumuliform clouds. *Quart. J. Roy. Meteor. Soc.,* **117,** 207–241.
——, and ——, 2001: Ice particles in stratiform clouds in the Arctic and possible mechanisms for the production of high ice concentrations. *J. Geophys. Res.,* **106** (D14), 15 065–15 075.
Rogers, D. C., 1982: Field and laboratory studies of ice nucleation in winter orographic clouds. Ph.D. dissertation, University of Wyoming, Laramie, WY, 161 pp.
——, 1994: Detecting ice nuclei with a continuous flow diffusion chamber—Some exploratory tests of instrument response. *J. Atmos. Oceanic Technol.,* **11,** 1042–1047.
——, P. J. DeMott, and L. O. Grant, 1994: Concerning primary ice concentration and water supersaturations in the atmosphere. *Atmos. Res.,* **33,** 151–168.
——, ——, S. M. Kreidenweis, and Y. Chen, 1998: Measurements of ice nucleating aerosols during SUCCESS. *Geophys. Res. Lett.,* **25,** 1383–1386.
——, ——, and ——, 2001: Airborne measurements of tropospheric ice-nucleating aerosol particles in the Arctic spring. *J. Geophys. Res.,* **106,** 15 053–15 063.
Sassen, K., 1989: Reply. *J. Atmos. Sci.,* **46,** 2346–2347.
——, and G. C. Dodd, 1988: Homogeneous nucleation rate for highly supercooled cirrus cloud droplets. *J. Atmos. Sci.,* **45,** 1357–1369.
——, and ——, 1989: Haze particle nucleation simulation in cirrus clouds, and application for numerical and lidar studies. *J. Atmos. Sci.,* **46,** 3005–3014.
——, and S. Benson, 2000: Ice nucleation in cirrus clouds: A model study of the homogeneous and heterogeneous nucleation modes. *Geophys. Res. Lett.,* **27,** 521–524.
——, P. J. DeMott, J. M. Prospero, and M. R. Poellot, 2003: Saharan dust storms and indirect aerosol effects on clouds: CRYSTAL–FACE results. *Geophys. Res. Lett.,* **30,** 1633, doi:10.1029/2003GL017371.
Sedunov, Y. S., 1974: *Physics of Drop Formation in the Atmosphere.* Wiley, 234 pp.
Spice, A., D. W. Johnson, P. R. A. Brown, A. G. Darlison, and C. P. R. Saunders, 1999: Primary ice nucleation in orographic cirrus cloud: A numerical simulation of the microphysics. *Quart. J. Roy. Meteor. Soc.,* **125,** 1637–1667.
Starr, D. O'C., and Coauthors, 2000: Comparison of cirrus cloud models: A Project of the GEWEX Cloud System Study (GCSS) Working Group on Cirrus Cloud Systems. *Proc. Int. Cloud Physics. Conf.,* Reno, NV, ICCP, 1–4.
Uttal, T., and Coauthors, 2002: Surface heat budget of the Arctic Ocean. *Bull. Amer. Meteor. Soc.,* **83,** 255–276.
Young, K. C., 1974: The role of contact nucleation in ice phase initiation in clouds. *J. Atmos. Sci.,* **31,** 768–780.
——, 1993: *Microphysical Processes in Clouds.* Oxford University Press, 427 pp.
Yum, S. S., and J. G. Hudson, 2001: Vertical distributions of cloud condensation nuclei spectra over the springtime Arctic Ocean. *J. Geophys. Res.,* **106** (D14), 15 045–15 052.